

**Citation for published version:**

Pushp Raj Tiwari, et al, 'Simulations of Tropical Circulation and Winter Precipitation Over North India: an Application of a *Tropical Band Version* of Regional Climate Model (RegT-Band)', *Pure and Applied Geophysics*, Vol. 173 (2): 657-674, February 2016.

**DOI:**

<https://doi.org/10.1007/s00024-015-1102-1>

**Document Version:**

This is the Accepted Manuscript version.

The version in the University of Hertfordshire Research Archive may differ from the final published version. **Users should always cite the published version.**

**Copyright and Reuse:**

© Springer Basel 2015.

This manuscript version is distributed under the terms of the Creative Commons Attribution licence (<http://creativecommons.org/licenses/by/4.0/>), which permits unrestricted re-use, distribution, and reproduction in any medium, provided the original work is properly cited.

**Enquiries**

If you believe this document infringes copyright, please contact the Research & Scholarly Communications Team at [rsc@herts.ac.uk](mailto:rsc@herts.ac.uk)

**Simulations of tropical circulation and winter precipitation over north India: An application of a tropical band version of Regional Climate Model (RegT-Band)**

P. R. Tiwari<sup>1</sup>, S.C.Kar<sup>2\*</sup>, U.C.Mohanty<sup>3</sup>, S.Dey<sup>1</sup>, S. Kumari<sup>1</sup>, P. Sinha<sup>1</sup>, P. V. S. Raju<sup>4</sup>

and M.S. Shekhar<sup>5</sup>

<sup>1</sup>Centre for Atmospheric Sciences, IIT Delhi, India

<sup>2</sup>National Centre for Medium Range Weather Forecasting, Noida, India

<sup>3</sup>School of Earth Ocean and Climate Sciences, IIT Bhubaneswar, India

Center of Excellence for Climate Change Research, King Abdulaziz University, Saudi Arabia

<sup>5</sup>Research and Development Centre, Snow and Avalanche Study Establishment, Chandigarh,  
India

---

\*Correspondence

Dr. S. C. Kar

National Centre for Medium Range Weather Forecasting (NCMRWF),

A-50, Sector-62, Noida, India

[sckar@ncmrwf.gov.in](mailto:sckar@ncmrwf.gov.in)

## **Abstract**

In the present study, simulations have been carried out to study the relationship between wintertime precipitations and the large scale global forcing (ENSO) using the tropical band version of Regional Climate Model (RegT-Band) for 5 El Niño and 4 La Niña years. The RegT-Band model is integrated with the observed sea-surface temperature and lateral boundary conditions from National Center for Environmental Prediction (NCEP)-Department of Energy (DOE) reanalysis 2 (NCEP-DOE2) reanalysis. The model domain extends from 50° S to 50° N and covers the entire tropics at a grid spacing of 45 km, i.e. it includes lateral boundary forcing only at the southern and northern boundaries. The performance evaluation of the model in capturing the large scale fields followed by ENSO response with wintertime precipitation has been carried out by using model simulations against NCEP-DOE2 and Global Precipitation Climatology Project (GPCP) precipitation data. The analysis suggests that the model is able to reproduce the upper airfields and large-scale precipitation during wintertime, although the model has some systematic biases compared to the observations. A comparison of model-simulated precipitation with observed precipitation at 17 station locations has been carried out. It is noticed that the RegT-Band model simulations are able to bring out the observed features reasonably well. Therefore, this preliminary study indicates that the tropical band version of the regional climate model can be effectively used for the better understanding of the large-scale global forcings.

Key words: Winter precipitation, ENSO, RegT-Band.

## 1. Introduction

Precipitation over the north Indian region ( $23^{\circ}$  N –  $37^{\circ}$  N and  $60^{\circ}$  E - $90^{\circ}$  E) during winter seasons (December, January and February - DJF) has profound socio-economic impacts. Precipitation during winter occurs in this region mainly due to passage of Western Disturbances (WDs) (Pisharoty and Desai 1956; Mooley 1957) across north India from the west to east (Dutta and Gupta 1967; Singh and Kumar 1977; Agnihotri and Singh 1982). During winters, most of the precipitation is concentrated over this region in the form of rain in the plains and snow at higher altitudes (Mohanty *et al.* 1999).

There is significant interannual variation of precipitation amount over north India during winter season. Apart from the WDs, the hydrodynamic and thermodynamic instabilities during winter season are major indicator for the precipitation over this region (Dimri 2013). The winter precipitation is major source over north India for water management and agricultural planning. Therefore, prior information on seasonal scale winter precipitation will be helpful for effective planning in various sectors. Many studies reported that summer monsoon precipitation influenced by large scale forcing of Hadley cell and El Nino- southern oscillation (ENSO) events (Kripalani *et al.* 1997; Ihara *et al.* 2007). On the other hand, limited studies on the association of the winter precipitation and large-scale fields (Krishna Kumar *et al.* 1999; Mariotti 2007; Yadav *et al.* 2010; Kar and Rana 2013). Yadav *et al.* (2010) suggested that the WDs intensify over northwest India due to a baroclinic response to a large-scale sinking motion over the western Pacific during the warm phase of ENSO that causes an upper-level cyclonic circulation anomaly north of India and a low-level anti-cyclonic anomaly over southern and central India. Kar and Rana (2013) found that the two dominant modes of interannual variability of zonal wind at 200

hPa of Northern Hemisphere winter were similar to that of ENSO and North Atlantic oscillation (NAO)/ Arctic Oscillation (AO) patterns respectively. The correlation of northwest India and adjoining (NWIA) precipitation with the ENSO mode is larger than its correlation with the NAO or AO modes.

Therefore, a detail investigation with observational and numerical studies to understand the large-scale effects/teleconnections of ENSO during winter season over north India will provide insight into the predictability of precipitation over this region. In view of the relative absence of studies exploring the forces driving winter precipitation, the present study examines this precipitation regime as a response to the well-known determining factors to enhance forecasting abilities.

Tiwari *et al.* (2014) have examined the performance of Regional climate model version 4 (RegCM4) in simulating the wintertime circulation and precipitation patterns over northwest India with reasonable success. In such models for the region, impacts of SST variability occurring elsewhere (outside the domain) are included through lateral boundary conditions. The tropical band version of RegCM (Coppola *et al.* 2012) (hereafter referred to as RegT-Band) gives the possibility to run the model on global scale. Till now, only a few regional climate models (RCMs) have been run in such a configuration (Tulich *et al.* 2010; Murthi *et al.* 2011; Ray *et al.* 2011). RegT-Band offers the opportunity to explore a range of processes related to tropical climate interactions and to assess the performance of given physics parameterizations in a wide range of climate contexts (Ju and Slingo 1995; Giannini *et al.* 2003; Rauscher *et al.* 2010; Mariotti *et al.* 2011). In addition, in a tropical band configuration, the domain of the RCM model is large in terms of its longitudinal extent. There is no requirement of lateral boundary conditions

along zonal direction. Therefore, the processes within the domain (i.e. in the area of interest) are less strongly influenced by the lateral boundary conditions (LBCs), however this does not happen in a typical limited area configuration. The RegT-Band model performance reflects its ability to simulate large-scale circulations and processes not strongly forced by the lateral meteorological boundary conditions, as in traditional RCM experiments. In this regard, the tropical band RCM might behave more as a global model than as a regional one. On the other hand, the comparison with results from corresponding traditional RCM experiments over domains encompassed by the tropical band can provide useful information on the effects of the lateral boundary forcing in limited area domains. It should be stressed that the RegCM system of this kind is not used till now for studying the role of ENSO on winter precipitation over northwest India, so can provide information if this model is able to simulate this relationship. As the RegT-Band model covers entire tropical domain, examination of its skill in simulating the role of ENSO on the wintertime precipitation over north India becomes important in the context of mechanism proposed by Yadav *et al.* (2010) and Kar and Rana (2013). Therefore, for this study, wintertime simulations to diagnose ENSO influences using RegT-Band model have been chosen.

In following paragraphs, Section 2 illustrates data and methodology used in the present study followed by results and discussion in Section 3. Finally, Section 4 brings out salient features out of this study under conclusions.

## **2. Description of the Model, data used and Methodology**

**2.1 Model:** The regional climate model (RegCM4, version 4.1.1), developed at the International

Centre for Theoretical Physics, Italy, consists of hydrostatic dynamical core similar to the version of the Mesoscale Model (MM5) (Grell *et al.* 1994). The model has 18 vertical sigma levels in which five levels are in the lower troposphere (Giorgi *et al.* 1989; Pal *et al.* 2007) in its standard configuration. It is a hydrostatic, terrain following model with state-of-the-art physical parameterization schemes. The model can be configured by choosing physics options from among multiple schemes. The details of the other configurations including physical parameterization schemes in the model can be found in Pal *et al.* (2007). For the present experiment we use the following model configuration, which is given in Table 1.

The tropical band configuration (Coppola *et al.* 2012) implemented in the present work uses a Mercator projection horizontal grid with the grid interval:

$$R_x = \frac{2\rho r}{n} \dots\dots\dots(i)$$

where  $n$  is the number of grid points in an east-west direction and  $r$  is the radius of the Earth. With this choice of  $R_x$ , the end points at the eastern and western boundaries exactly overlap; therefore, if periodic lateral boundary conditions are used in an east-west direction, a continuous field is obtained for a tropical band encompassing the entire Earth's circumference. For our experiments we have chosen a grid interval of 45 km. The domain with control height of the model is shown in Figure 1.

**2.2 Data and Methodology:** In this study, model forcing conditions at the northern and southern boundaries are obtained from the NCEP-DOE2 reanalysis (Kanamitsu *et al.* 2002) available at 2.5°×2.5° resolution (hereafter referred to as NNRP2), SSTs at the lower boundary are taken

from National Oceanic and Atmospheric Administration Optimal Interpolation SST (version 2, NOAA\_OISST\_V2) available at  $1^{\circ} \times 1^{\circ}$  resolution (Reynolds *et al.* 2002) and the geophysical parameters are provided by United States of Geophysical Survey (USGS) at 10' resolution. Observed data used for the model validation include the Global Precipitation Climatology Project daily precipitation dataset (GPCP,  $2.5^{\circ} \times 2.5^{\circ}$  resolution; Alder *et al.* 2003), Tropical Rainfall Measuring Mission (TRMM,  $0.25^{\circ} \times 0.25^{\circ}$  resolution daily precipitation product; Kummerow *et al.* 2001, Huffman *et al.* 2007), India Meteorological Department (IMD) gridded ( $1^{\circ} \times 1^{\circ}$ ) precipitation data (Rajeevan *et al.* 2006) and CRU (Harris *et al.* 2013) surface air temperatures. Observed seasonal precipitation data obtained from Snow and Avalanche Study Establishment (SASE) for seventeen stations over the western Himalaya (Fig. 18) is also used to validate the model results at station locations. In addition to the above, global reanalysis data have been used in the present study. These are the NNRP2 atmospheric and surface fields, ERA-Interim reanalysis (Dee *et al.* 2011).

Composite analysis and correlation maps are prepared to understand the variability of various meteorological parameters. We have categorized, warm and cold phases of ENSO for the period 1983 to 2010 based on Standard deviation. i.e., above (below) one standard deviation of SOI index over NINO 3.4 region is considered as El Nino (La Nina) years. Based on [www.cpc.ncep.noaa.gov/products/precip/CWlink/MJO/enso.shtml](http://www.cpc.ncep.noaa.gov/products/precip/CWlink/MJO/enso.shtml), five El Niño years (1987-88, 1991-92, 1997-98, 2002-03, 2009-10) and four La Niña years (1988-89, 1998-99, 2000-01, 2007-08) are considered for preparing a set of two composites for comparisons. Therefore, in total, 9 years (5 El Niño years and 4 La Niña years) of model simulations have been used for the analysis in the present study. An effort has been made to explore the linkages between global

SST and observed area averaged winter rainfall over north India by using the composite maps for the El Niño and La Niña years. The SST data used is obtained from NOAA ERSSTv3b extended reconstructed monthly sea-surface temperature dataset for the whole globe (Smith *et al.* 2008).

The model is integrated from November 1<sup>st</sup> to February 28<sup>th</sup> (29<sup>th</sup> for leap year) for each ENSO year. Model simulations from December to February are used in this study after considering the simulations of the first month as spin up time of the model. The model integration is carried out at horizontal resolution of 45 km.

### **3. Results and Discussions**

The results obtained from the RegT-Band model simulations are analyzed in two broad sections. In the first section, upper air circulation features and precipitation distribution are described for the tropics while in the next section the above said feature are analyzed for the north India. For the sake of brevity, composite plots of upper air fields and precipitation from the RegT-Band simulations are presented here. The Student's t-test is applied for statistical significance for differences in composite plots, and the critical value is 2.8 at 10% significance level.

#### **3.1 Circulation features**

The RegT-Band model simulated results have been analyzed to examine the upper air circulation patterns for El Niño and La Niña years. For this purpose, the model simulated upper air wind and precipitation fields are compared with NNRP2 reanalysis and IMD datasets. The seasonal mean (DJF) composite wind (El Niño, La Niña and El Niño minus La Niña) at 500 hPa

from verification analysis (NNRP2) and model simulations are shown in Figure 2 and 3 respectively. The composite plots shows that in the case of El Niño and La Niña years (Fig. 2), strong westerly winds spread from Iran to the Himalayan region. However, the spatial extent and the wind strength is less in the La Niña years. The difference of composite winds for of El Niño and La Niña years show a cyclonic flow near  $160^{\circ}$  E -  $120^{\circ}$  W/  $25^{\circ}$  N -  $45^{\circ}$  N. RegT-Band simulated composite wind fields are shown in Fig. 3. The figure shows that in case of El Niño and La Niña years, the model is able to depict the observed features up to certain extent, however the simulated wind fields have more spatial extent and higher strength. In the case of El Niño minus La Niña year composite there is a cyclonic flow but it is shifted eastward and has the less strength. From the difference plots in Fig. 2 (c) & 3 (c), it is seen that, when this cyclonic flow is hindered by the Himalayas, it intensifies precipitation over the hilly regions and adjoining plains.

### **3.2 Spatial distribution of precipitation**

In order to understand the skill of the RegT-Band model in simulating precipitation distribution and intensity, seasonal mean composite precipitation (DJF) for El Niño and La Niña years have been analyzed and shown in figure 4 and 5. A precipitation band can be seen in Fig. 4 (a) along equator and  $15^{\circ}$  S with maximum intensity between  $170^{\circ}$  E -  $130^{\circ}$  W in observation. This observed feature is brought out well by the model, Fig. 4 (b), though with lower intensity. The difference between the model simulated and observed precipitation is shown in Fig. 4 (c). It is seen that there is a positive bias over the Indian Ocean and along the equator. Observed seasonal (DJF) mean composite precipitation for La Niña years shown in Fig 5 (a) indicate that the precipitation band is between the equator and  $15^{\circ}$  S and its intensity is more over the Indian

Ocean, South African and American region. The RegT-Band model simulated precipitation is shown in the Fig. 5 (b). It is seen that the model is able to delineate this observed feature reasonably well but with lesser spatial extent of precipitation. It is also seen that there is a northward shift in the precipitation along eastern coast of India and more intense precipitation over southern regions of Africa in the model compared to the observation. The difference between model simulated precipitation and observation in Fig. 5 (c) shows that there is a positive bias over the Indian Ocean and southeastern parts of Africa.

Fig. 6 depicts the observed and model simulated composite seasonal mean precipitation difference (El Niño minus La Niña years). This difference is positive in the Niño region especially over the Niño 4 and 3.4 regions. Over the Indian Ocean region, the difference is negative. The RegT-Band simulation (Fig. 6b) is able to delineate some of the observed precipitation features spatially however the strength is very less. The model is also not able to bring out the precipitation features over the Niño regions, which is a major flaw of the model. Overall, it is noticed from the difference composites for the season (DJF) that there is an increase in rainfall ( $\sim 2$  mm day<sup>-1</sup>) over north India and southeastern parts of Africa due to ENSO forcing.

In order to examine how well did the distribution of model simulated precipitation values correspond to the distribution of observed values, a box-whisker plot has been drawn for global as well as for domain of interest for El Niño and La Niña years and shown in Fig. 7. The boxes indicate the 25<sup>th</sup> to 75<sup>th</sup> percentiles of the distribution, while the whiskers show the full width of the distribution. In case of both El Niño and La Niña years for global and region-specific

precipitation, it can be noticed that the distribution of the model-simulated values are comparable to the distribution of observed values, however, they are on higher side.

### **3.3 Tropical circulation from observation and model simulations**

In lower latitudes the strong driving forces of the general circulation are large-scale tropical circulations such as Walker and Hadley circulations (Tanaka *et. al.* 2004; Pillai 2008). Therefore, to assess the model capability in capturing the equatorial east-west Walker circulation, we have plotted the vertical profile of  $u$  (zonal wind) and vertical velocity ( $\omega$ ) averaged over  $10^{\circ}\text{S} - 10^{\circ}\text{N}$ . Fig. 8 (a) shows the observed Walker cell in which upward motion is seen over the Indian Ocean. Fig. 8 (b) shows the model simulated Walker cell in which the strength of the rising motion in the western pacific is more and the region of rising motion is extending up to date line at lower levels as compared to observation. To assess the models capability in capturing the north-south Hadley circulation the meridional wind (vertical profile of  $v$ ) and vertical velocity ( $\omega$ ) averaged over  $28^{\circ}\text{E} - 128^{\circ}\text{E}$  is shown in Fig. 9. The rising motion is observed over north of the equator and sinking motion between  $25^{\circ}\text{N}$  to  $40^{\circ}\text{N}$ . The model is able to simulate the rising and sinking motion reasonably well. However the strength of ascending and descending cells is less than that is observed.

Further, Fig. 10 compares the zonally averaged surface air temperature for the El Niño year (2009-10) between latitudinal belt of  $50^{\circ}\text{S} - 50^{\circ}\text{N}$  in CRU, ERA-Interim and RegT-Band simulation. For the seasonal mean of DJF, the RegT-Band model shows good agreement with observations north of  $40^{\circ}\text{N}$ , while it underestimates the surface air temperature by about  $3^{\circ}\text{C}$  between  $30^{\circ}\text{S}$  and  $25^{\circ}\text{N}$  compared to CRU and ERA-Interim observations. Similar behavior is

found for composite La Niña years (Figure not shown), with good agreement with observations north of 30°N and an underestimation in rest of the region.

### **3.4 Circulation over the domain of interest**

#### ***3.4.1 Zonal and meridional wind***

The composite vertical structures of the seasonal mean (DJF) zonal and meridional winds for the El Niño and La Niña years are shown in Fig. 11 and 12 respectively. Zonal and meridional components of wind have been averaged over the longitudinal belt from 28° E to 128° E. The latitudinal cross-section of the sectorial (28° E - 128° E) zonal and meridional wind from NNRP2, RegT-Band and RegT-Band minus observed experiments for El Niño and La Niña years are shown in Figure 11. It is seen that the upper air westerly jet stream (WJS) is well represented in the RegT-Band simulation. However, the area with core WJS in model simulation is shifted northward compared to the verification analysis in case of El Niño years. Sectorial (averaged over 28° E -128° E) meridional composite wind for El Niño years is also shown in Figure 11 (right panels). It reveals that the meridional winds at upper pressure levels (between 200-100 hPa) are stronger in the verification analysis as compared to the RegT-Band simulation. The locations of the stronger meridional winds are shifted northward in model simulation as compared to the verification analysis. Moreover, the strength is weaker in the case of model simulated meridional composite winds. The difference between the model and observation for zonal and meridional composite winds for El Niño years is shown in Fig. 11 (c & f). It is seen that the sectorial composite of zonal wind shows stronger winds ( $> 8 \text{ m sec}^{-1}$ ) at upper levels (above 400 hPa) from 35° N - 45° N. The difference between RegT-Band and observation in the

case of meridional composite winds in Fig. 11 (f) shows less strength compared to the sectorial composite of zonal wind at upper pressure levels.

The sectorial composite of zonal and meridional winds for La Niña years is shown in Fig. 12. The diagram indicates that the upper air westerly jet stream (WJS) is well represented in RegT-Band simulation, however, the area with core WJS in RegT-Band simulation is shifted northward about  $3^\circ$  compared to the verification analysis. The model simulated WJS are also stronger compared to the observation. Sectorial (averaged over  $28^\circ$  E -  $128^\circ$  E) meridional composite wind for La Niña years is shown in Figure 12 (right panels). It reveals that the meridional winds at upper levels (between 200-100 hPa) are stronger in the verification analysis compared to the RegT-Band simulation. The locations of the areas with stronger meridional winds are shifted northward in RegT-Band simulation as compared to the analysis, however, the strength is less in RegT-Band simulated meridional composite wind. The difference between RegT-Band and verification analysis for zonal and meridional composite wind for La Niña years is shown in Fig. 12 (c & f). In case of difference plot between RegT-Band and observation it is seen that the sectorial composite of zonal wind shows stronger winds ( $> 6 \text{ m sec}^{-1}$ ) at upper levels (above 400 hPa) from  $37^\circ$  N -  $45^\circ$  N. Overall, the spatial pattern and intensity of the zonal as well as meridional composite winds are represented well by the RegT-Band simulations.

### ***3.4.2 Vertical structure of the temperature***

A composite analysis of the vertical structures of the sectorial ( $28^\circ$  E -  $128^\circ$  E) seasonal mean (DJF) temperature has been made for the El Niño and La Niña years (Fig. 13). It is seen that during the El Niño and La Niña years, the RegT-Band is able to simulate the observed

temperature pattern well. The difference between RegT-Band and verification analysis for composite temperature for El Niño and La Niña years is shown in Fig. 13 (c & f). It is seen that the temperature is higher ( $> 2 \text{ }^{\circ}\text{K}$ ) at upper levels (between 400- 200 hPa) from  $29^{\circ}\text{N}$  -  $42^{\circ}\text{N}$ . The difference between RegT-Band and observation in the case of composite temperature for La Niña year's shows higher values compared to the composite El Niño years at upper levels that extends from  $25^{\circ}\text{N}$  -  $42^{\circ}\text{N}$ . Overall, the spatial pattern and intensity of the sectorial composite temperature for El Niño and La Niña years is represented well by the RegT-Band simulations.

### **3.5 Precipitation over north India**

In order to understand the skill of RegT-Band model in simulating the seasonal mean precipitation distribution and intensity over the north India, composite analysis has been carried out for El Niño and La Niña years (Fig. 14). The distribution and intensity of simulated precipitation is well represented by the RegT-Band model over north India for the composite El Niño and La Niña years. During El Niño years, it is noticed that the model is able to delineate the observed features up to certain extent, however, the spatial extent and amount is higher ( $> 5 \text{ mm day}^{-1}$ ) compared to the observations. On the other hand, for the La Niña years, the RegT-band simulated precipitation agrees well with the observations. However, the model simulates higher amount of precipitation ( $> 2 \text{ mm day}^{-1}$ ) compared to that in the observations.

The difference in RegT-Band simulated and observed precipitation is shown in Fig. 14 (c & f) for composite El Niño and La Niña years. In the case of El Niño years, a higher precipitation difference ( $> 3 \text{ mm day}^{-1}$ ) is seen compared to the La Niña years over the north India. This analysis indicates that during El Niño years, this region receives more precipitation

compared to La Niña years. This result agrees with observational studies of Yadav *et al.* (2009). Overall, the model has the capability to reproduce the observed features; however, the intensity of the simulated precipitation is on higher side. This may be due to strengthening of circulation associated with ENSO in the model simulations, and hence enhanced precipitation during the winter. Fig. 15 & 16 present the Hovmoller precipitation diagram based on daily (DJF) precipitation for the El Niño year (2009-10) and La Niña year (2000-01) over north India from TRMM and RegT-Band model simulations. This diagram illustrates the evolution of zonal cross-section of daily precipitation on intraseasonal time scale. It can be noticed in the Fig. 15 (a) that over north India, the precipitation band moves southward from about 30°-25°N till December, where it resides until mid-January and then starts moving northward. The RegT-Band (Fig. 15 b) clearly shows an overestimation of precipitation between mid-December and first week of February at low latitudes i.e. south of 30°N. Further, during the La Niña year, the RegT-Band model simulated precipitation band (Fig. 16 b) does reach up to 23°N during the mid-January, which is not seen in TRMM observations. Overall, the results indicate that the RegT-Band captures the daily evolution of the DJF precipitation over north India; however, it results in over estimation of precipitation compared to observations. This may be due to representation of convection as well as surface process in the model. Therefore, more testing is required to assess which model options and parameters can improve this problem.

Furthermore, to find out the teleconnection of north India winter precipitation to the zonal position of the El Nino warming, we have calculated the difference of observed SST for El Niño and La Niña years. Fig. 17 shows the core of maximum SST between 140°W and 110°W. The

other positive anomalies areas are northwest and south-central tropical Indian Ocean. This composite analysis confirms that whenever there is warmer SST, more precipitation is observed over the north India (Fig. 14).

### **3.6 Validation against station observations**

In this section, the RegT-Band simulated precipitation is validated against the observations over seventeen stations located over the Indian part of the Western Himalayas (IWH) region (Fig. 18). These observational datasets are made available by Snow and Avalanche Study Establishment (SASE). To validate the model gridded precipitation dataset to station level, a bi-linear interpolation method is applied to model data to obtain precipitation at station levels. Station-wise seasonal mean precipitation obtained from observations and model simulations are shown in Table 2. It is seen from the Table that performance of the RegT-Band model in simulating precipitation in El Niño and La Niña years is reasonably good and closer to observations. However, for most of the stations, the model shows a wet bias.

Based on the results of Table 2, the performance of the model has been evaluated through analyzing the variation in precipitation in El Niño and La Niña years. For this purpose, phase synchronizing events (PSE) have been computed. PSEs have been calculated using model output and observation for all the 17 stations of the SASE in the region. The PSE method matches the sign (positive or negative) of the precipitation difference (composite of El Niño minus composite of La Niña years) obtained from observations (data from SASE stations) and model simulations to evaluate the performance of the model.

The computation of PSE is as follows:

$$PSE = \frac{E - E'}{E} \times 100 \quad \dots\dots\dots(ii)$$

where  $E$  is the total number of events and  $E'$  is the number of events in model simulation that have opposite in sign as compared to observations (out of phase). Thus, PSE=100 for model results means that the sign of model anomalies (here the difference from composite of El Niño and La Niña years) is same as in the observations for all the stations and PSE=0 when none of the model results have a similar sign (i.e. either positive or negative both in model and observation) with observations. Using the results of Table 2, it is seen that the PSE value is the same (with 94%) for composite (i.e., model output matches the sign of with observations 94% times) of El Niño minus La Niña years. Therefore, it can be concluded that RegT-Band model simulations are able to represent the precipitation pattern and intensity with high fidelity.

#### 4. Conclusions

The skill of RegT-Band model at horizontal grid spacing of 45 km in simulating the large-scale effects/teleconnections of ENSO has been studied in the present work. For this, an assessment of capability of the model in simulating the large-scale fields (e.g. upper air wind and precipitation) for a composite of five El Niño and four La Niña years has been made. The ability of the RegT-Band model in capturing the wintertime precipitation over the north India has also been examined. The major findings, advantages of RegT-Band simulations and future scope of the study are as follows:

- The analysis presented here indicates that the RegT-Band model is able to reproduce the basic characteristics of the upper airfields and large-scale precipitation during wintertime, although with some systematic biases as compared to the observations. In the RegT-Band model it is found that there is a consistency between circulation and precipitation.
- RegT-Band model simulations are able to delineate the observed features of winds, temperature and precipitation over north India reasonably well. However, the precipitation amount simulated by the model is higher than the observed amount.
- To understand the model performance in simulating the precipitation at station locations over the Indian part of western Himalayas (IWH) region, phase synchronizing event (PSE) has been computed and it has been found that the RegT-Band model simulations are able to bring out the observed features with high fidelity for the El Niño and La Niña years.
- The main advantage of RegT-Band simulation is that within the computational domain, the impact of LBC is not large over the region of interest. Entire tropical circulation can also be simulated including the direct impact of ENSO and other tropical processes which can't be done in other Regional Models.

Although, for the present work, a particular set of El Niño and La Niña years has been selected, the results are encouraging for the use of the RegT-Band configuration for tropical climate process studies. In our future work, it is proposed to take up the issue of impact of ENSO on Indian Summer Monsoon Rainfall (ISMR) by using RegT-Band configuration.

## Acknowledgements

Snow and Avalanche Study Establishment (SASE) supported this study. The RegCM4.1.1 installed at IIT Delhi was developed at the Abdus Salam ICTP, Trieste, Italy. The authors acknowledge the National Center for Environmental Prediction (NCEP), Global Precipitation Climatology Project (GPCP) USA and India Meteorological Department for providing valuable data sets for accomplishing this work. The authors are thankful to Bianca C. for editing/correcting the English of the manuscript. We also thank the anonymous reviewers for their help in improving the earlier version of the manuscript.

## References

- Adler, R.F., G.J. Huffman, A. Chang, R. Ferraro, P. Xie, J. Janowiak, B. Rudolf, U. Schneider, S. Curtis, D. Bolvin, A. Gruber, J. Susskind, and P. Arkin, 2003: *The version 2 global precipitation climatology project (GPCP) monthly precipitation analysis (1979–Present)*. Journal of Hydrometeorol., 4, 1147–1167.
- Agnihotri, C.L., and M.S. Singh, 1982: *Satellite study of western disturbances*. *Mausam*. 33 (2), 249-254.
- Coppola E., F. Giorgi, L. Mariotti, and X. Bi, 2012: *RegT-Band: A tropical band version of RegCM4*. Clim. Res., 52, 115–133.
- Dee DP., S.M. Uppala, A.J. Simmons, P. Berrisford, P. Poli, S. Kobayashi, U. Andrae, M.A. Balmaseda, G. Balsamo, P. Bauer, P. Bechtold, A.C.M. Beljaars, L. van de Berg, J. Bidlot, N. Bormann, C. Delsol, R. Dragani, M. Fuentes, A.J. Geer, L. Haimberger, S.B. Healy, H. Hersbach, E.V. Hólm, L. Isaksen, P. Kållberg, M. Köhler, M. Matricardi, A.P.

- McNally, B.M. Monge-Sanz, J.J. Morcrette, B.K. Park, C. Peubey, P. de Rosnay, C. Tavalato, J.N. Thépaut, and F. Vitart, 2011: *The ERA-Interim reanalysis: configuration and performance of the data assimilation system*. Q.J.R. Meteorol. Soc., *137*, 553–597.
- Dimri, A.P., 2013: *Relationship between ENSO phases with Northwest India winter precipitation*. Int. J. Climatol., *33*, 1917–1923.
- Dutta, R.K., and M.G. Gupta, 1967: *Synoptic study of the formation and movement of western depressions*. Indian J. Meteorol. Geophys., *18*, 45-50.
- Fritsch, J.M., and C.F. Chappell, 1980: *Numerical prediction of convectively driven mesoscale pressure systems, part I: Convective parameterization*. J. Atmos. Sci., *37*, 1722–1733.
- Grell, G. A., 1993: *Prognostic evaluation of assumptions used by cumulus parameterization*. Mon. Wea. Rev., *121*, 764–787.
- Grell, G.A., J. Dudhia, and D.R. Stauffer, 1994: *Description of the fifth generation Penn State/NCAR Mesoscale Model (MM5)*. Tech Rep TN-398+STR, NCAR, Boulder Colorado, pp. 1-121.
- Giannini, A., R. Saravanan, P. Chang, 2003: *Oceanic forcing of Sahel rainfall on an interannual to interdecadal time scale*. Science. *302*, 1027–1030.
- Giorgi, F., and G.T. Bates, 1989: *The climatological skill of a regional model over complex terrain*. Mon. Wea. Rev., *117*, 2325–2347.
- Harris, I., P.D. Jones, T.J. Osborn, and D.H. Lister, 2014: *Updated high-resolution grids of monthly climatic observations – the CRU TS3.10 Dataset*. Int. J. Climatol., *34*, 623–642.
- Holtslag, A., E. DeBruijn, and H.L. Pan, 1990: *A high-resolution air mass transformation model for short-range weather forecasting*. Mon. Wea. Rev., *118*, 1561–1575.

- Huffman, G.J., D.T. Bolvin, E.J. Nelkin, D.B. Wolff, and others, 2007: *The TRMM multisatellite precipitation analysis (TMPA): quasi-global, multiyear, combined-sensor precipitation estimates at fine scale*. J. Hydrometeorol. 8, 38-55.
- Ihara, C., Y. Kushnir, M.A. Cane, and V.H. De La Pen˜a, 2007: *Indian summer monsoon rainfall and its link with ENSO and Indian Ocean climate indices*. Int. J. Climatol., 27, 179–187.
- Ju, J., and J.M. Slingo, 1995: *The Asian summer monsoon and ENSO*. Q. J. R. Meteorol. Soc., 121, 1133-1168.
- Kanamitsu, M., W. Ebisuzaki, J. Woollen, S.Y. Yang, J.J. Hnilo, M. Fiorino, and G.L. Potter, 2002: *NCEP-DEO AMIP-II Reanalysis (R-2)*. Bull. Am. Met. Soc., 83, 1631-1643.
- Kar, S.C., and S. Rana, 2014: *Interannual variability of winter precipitation over northwest India and adjoining region: impact of global forcing's*. Theor. Appl. Climatol., DOI 10.1007/s00704-013-0968-z.
- Kiehl, J.T., J.J. Hack, G.B. Bonan, B.A. Boville, B.P. Briegleb, D.L. Williamson, and P.J. Rasch, 1996: *Description of the NCAR Community Climate Model (CCM3)*. NCAR Tech. Note NCAR/TN- 420+STR, 152 pp.
- Kripalani, R.H., and A. Kulkarni, 1997: *Climatic impact of El Nino/La Nina on the Indian monsoon: a new perspective*. Weather. 52, 39–46.
- Krishna Kumar, K., B. Rajagopalan, and A. Cane, 1999: *On the weakening relationship between the Indian monsoon and ENSO*. Science. 284, 2156–2159.

- Kummerow C., Y. Hong, W.S. Olson, S. Yang, and others, 2001: *The evolution of the Goddard profiling algorithm (GPROF) for rainfall estimation from passive microwave sensors*. J Appl. Meteorol. 40,1801-1840.
- Mariotti, A., 2007: *How ENSO impacts precipitation over southwest central Asia?* Geophys. Res. Lett., 34, L16706.
- Mariotti, L., E. Coppola, M.B. Sylla, F. Giorgi, and C. Piani, 2011: *Regional climate model simulation of projected 21st century climate change over an all-Africa domain: comparison analysis of nested and driving model results*. J. Geophys. Res., 116, D15111. doi:10.1029/2010JD015068.
- Mooley, D.A., 1957: *The role of western disturbances in the production of weather over India during different seasons*. Indian J. Meteorol. Geophys., 8, 253-260.
- Murthi, A., K.P. Bowman, and L.R. Leung, 2011: *Simulations of precipitation using NRCM and comparisons with satellite observations and CAM: annual cycle*. Clim. Dyn., 36,1659-1679.
- Oleson, K. W., and coauthors, 2008: *Improvements to the Community Land Model and their impact on the hydrological cycle*. J. Geophys. Res., 113, G01021, doi:10.1029/2007JG000563.
- Pal, J.S., F. Giorgi, X. Bi, N. Elguindi, F. Solmon, X. Gao, S.A. Rauscher, R. Francisco, A. Zakey, J. Winter, M. Ashfaq, F. Syed, S. Faisal, J.L. Bell, N.S. Diffenbaugh, J. Karmacharaya, A. Konare, D. Martinez, R.P. Da Rocha, L.C. Sloan, and A.L. Steiner, 2007: *Regional climate modeling for the developing world: The ICTP RegCM3 and RegCNET*. Bull. Amer. Meteor. Soc., 88, 1395–1409.

- Pillai, P.A., 2008: *Studies on the role of tropospheric biennial oscillation in the interannual variability of Indian summer monsoon*. Ph.D dissertation, Cochin University of Science and Technology, 167 pp.
- Pisharoty, P., and B.N. Desai, 1956: *Western disturbances and Indian weather*. Indian J. Meteorol. Geophys., 8, 333-338.
- Rajeevan, M., J. Bhate, J. Kale, and B. Lal, 2006: *High-resolution daily gridded rainfall data for the Indian region: analysis of break and active monsoon spells*. Curr. Sci., 91, 296-306.
- Rauscher, S.A., F. Kucharski, and D.B. Enfield, 2010: *The role of regional SST warming variations in the drying of Meso-America in future climate projections*. J. Clim., 24, 2003-2016.
- Ray, P., C. Zhang, M.W. Moncrieff, J. Dudhia, J.M. Caron, L.R. Leung, and C. Bruyere, 2011: *Role of the atmospheric mean state on the initiation of the Madden Julian oscillation in a tropical channel model*. Clim. Dyn., 36,161-184.
- Reynolds, R.W., N.A. Rayner, T.M. Smith, D.C. Stokes, and W. Wang, 2002: *An improved in situ and satellite SST analysis for climate*. J. Climate., 15, 1609-1625.
- Singh, M.S., and S. Kumar, 1977: *Study of western disturbances*. Indian J. Meteorol. Geophys., 28(2), 233-242.
- Smith, T.M., R.W. Reynolds, C.P. Thomas, and J. Lawrimore, 2008: *Improvements to NOAA's Historical Merged Land-Ocean Surface Temperature Analysis (1880-2006)*. J. Climate., 21, 2283-2296.

- Tanaka, H.L., N. Ishizaki, and A. Kitoh, 2004: *Trend and inter-annual variability of Walker, monsoon and Hadley circulations defined by velocity potential in the upper troposphere. Tellus., 56 (A), 250–269.*
- Tawfik, A.B., and A.L. Steiner, 2011: *The role of soil ice in land-atmosphere coupling over the United States: a soil moisture precipitation winter feedback mechanism. J Geophys Res 116, D02113. doi:10.1029/2010JD014333.*
- Tiwari, P.R., S.C. Kar, U.C. Mohanty, S. Dey, P. Sinha, P.V.S. Raju, and M.S. Shekhar, 2014: *Dynamical downscaling approach for wintertime seasonal scale simulation over the Western Himalayas. Acta Geophys., 62 (4), 930-952.*
- Tulich, S.N., G.N. Kiladis, and A.S. Parker, 2010: *Convectively-coupled Kelvin and easterly waves in a regional climate simulation of the tropics. Clim. Dyn., 36, 185-203.*
- Yadav, R.K., K. Rupa Kumar, and M. Rajeevan, 2009: *Increasing influence of ENSO and decreasing influence of AO/NAO in the recent decades over northwest India winter precipitation. J. of Geophys.Res., 114, D12112, doi:10.1029/2008JD011318, 1-12.*
- Yadav, R.K., J.H. Yoo, F. Kucharski, and M.A. Abid, 2010: *Why Is ENSO Influencing Northwest India Winter Precipitation in Recent Decades? J. Climate., 23, 1979-1993.*

## List of Tables

Table 1. Configuration of RegT-Band model used in the present study.

Table 2. Seasonal Mean precipitation over seventeen (17) stations obtained from SASE observation and RegT-Band simulations for El Niño and La Niña years.

## List of Figures

Figure 1. The domain with control height (in m) of the model.

Figure 2. Observed seasonal mean composite wind (in  $\text{m sec}^{-1}$ ) at 500 hPa for DJF in (a) El Niño (b) La Niña and (c) El Niño minus La Niña years.

Figure 3. RegT-Band simulated seasonal mean composite wind (in  $\text{m sec}^{-1}$ ) at 500 hPa for DJF in (a) El Niño (b) La Niña and (c) El Niño minus La Niña years.

Figure 4. Seasonal mean composite (El Niño years) precipitation (in  $\text{mm day}^{-1}$ ) for DJF in (a) GPCP (b) RegT-Band and (c) difference between RegT-Band and GPCP.

Figure 5. Seasonal mean composite (La Niña years) precipitation (in  $\text{mm day}^{-1}$ ) for DJF in (a) GPCP (b) RegT-Band and (c) difference between RegT-Band and GPCP.

Figure 6. Seasonal mean composite (El Niño minus La Niña years) precipitation difference (in  $\text{mm day}^{-1}$ ) for DJF in (a) GPCP and (b) RegT-Band.

Figure 7: Distributions of observed and RegT-Band model simulated precipitation ( $\text{mm/day}$ ) for El Niño and La Niña years.

Figure 8. Composite (El Niño years) of Omega (vertical velocity) and zonal wind at pressure levels 1000 to 100 hPa for (a) Observation, (b) RegT-Band during DJF to show the Walker circulation represented by zonal wind and omega (multiplied by 600) averaged between 10<sup>0</sup>S and 45<sup>0</sup>N.

Figure 9. Composite (El Niño years) of Omega (vertical velocity) and meridional wind at pressure levels 1000 to 100 hPa for (a) Observation, (b) RegT-Band during DJF to show the Hadley circulation represented by meridional wind and omega (multiplied by 600) averaged between 28<sup>0</sup>E and 128<sup>0</sup>E.

Figure 10. Seasonal mean (DJF) zonally averaged surface air temperature for composite El Niño years.

Figure 11. Sectorial (28<sup>0</sup>E-128<sup>0</sup>E) zonal seasonal mean composite wind (in m sec<sup>-1</sup>) (a) Observed, (b) RegT-Band, (c) RegT-Band minus observed precipitation; Sectorial (28<sup>0</sup>E -128<sup>0</sup>E) meridional seasonal mean composite wind (in m sec<sup>-1</sup>) (d) Observed, (e) RegT-Band and (f) RegT-Band minus observed precipitation for El Niño years.

Figure 12. Sectorial (28<sup>0</sup>E-128<sup>0</sup>E) zonal seasonal mean composite wind (in m sec<sup>-1</sup>) (a) Observed, (b) RegT-Band, (c) RegT-Band minus observed precipitation; Sectorial (28<sup>0</sup>E -128<sup>0</sup>E) meridional seasonal mean composite wind (in m sec<sup>-1</sup>) (d) Observed, (e) RegT-Band and (f) RegT-Band minus observed precipitation for La Niña years.

Figure 13. Sectorial (28<sup>0</sup>E-128<sup>0</sup>E) zonal and meridional seasonal mean composite temperature (in <sup>0</sup>K) (a) Observed, (b) RegT-Band, (c) RegT-Band minus observed precipitation for El

Niño years; (d) Observed, (e) RegT-Band and (f) RegT-Band minus observed precipitation for La Niña years.

Figure 14. Seasonal mean composite precipitation (in  $\text{mm day}^{-1}$ ) (a) Observed, (b) RegT-Band, (c) RegT-Band minus observed precipitation for El Niño years; (d) Observed, (e) RegT-Band and (f) RegT-Band minus observed precipitation for La Niña years.

Figure 15. Hovmoller precipitation diagram for the El Niño year (2009-10) over the north India for (a) TRMM and (b) RegT-Band model.

Figure 16. Hovmoller precipitation diagram for the La Niña year (2000-01) over the north India for (a) TRMM and (b) RegT-Band model.

Figure 17. Seasonal mean (DJF) composite (El Niño minus La Niña years) for observed SST (in  $^{\circ}\text{C}$ ).

Figure 18. Seventeen station locations obtained from Snow and Avalanche Stud Establishment (SASE). These station observations of precipitation are used for validation of model results.

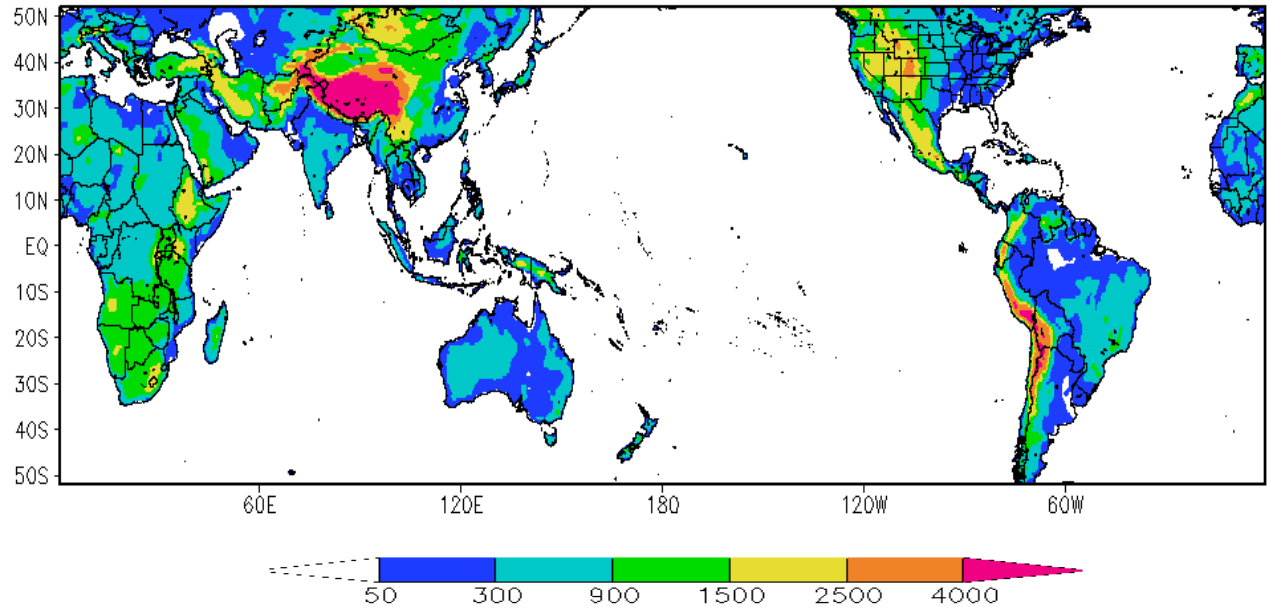


Figure 1: The domain with control height (in m) of the model.

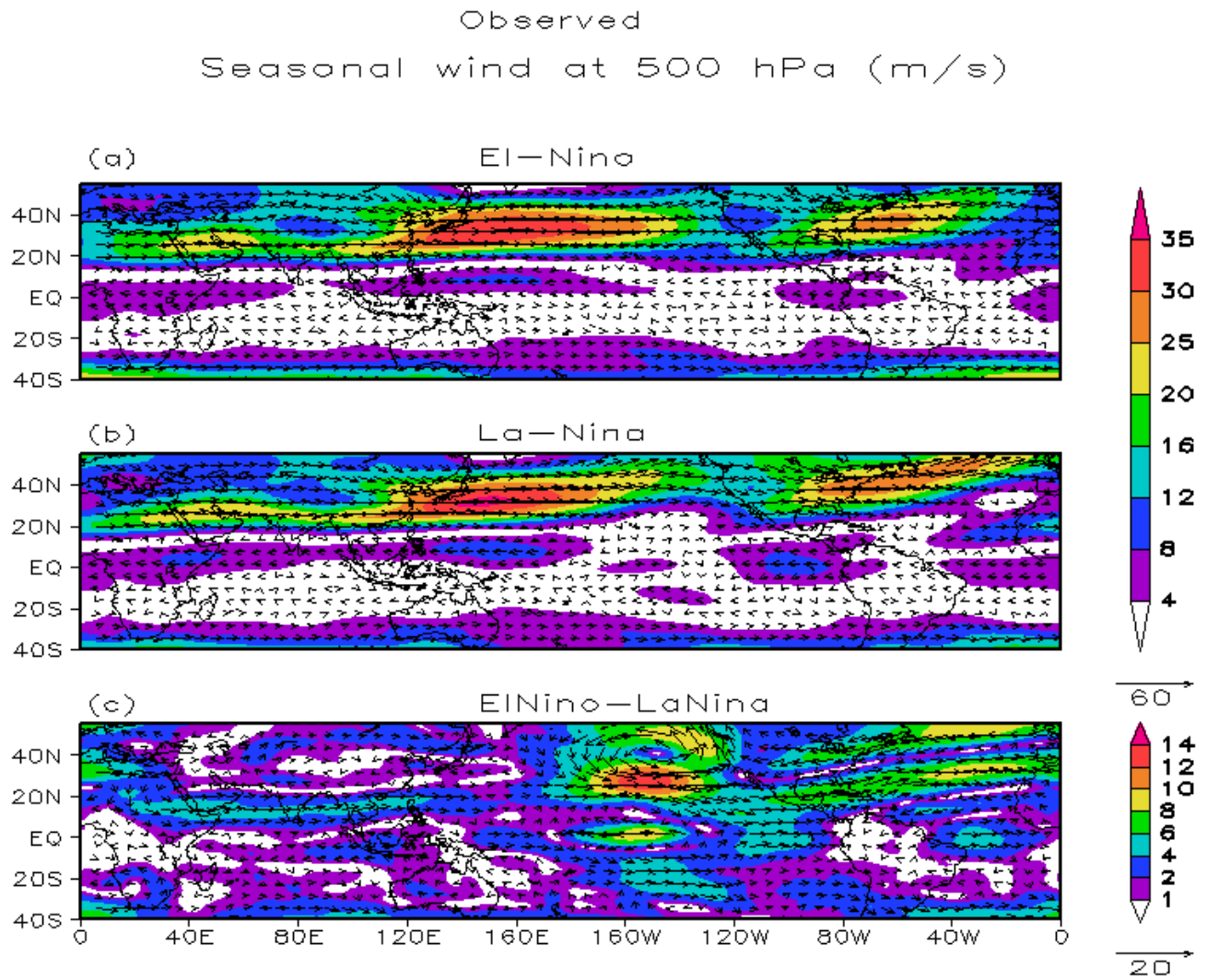


Figure 2: Observed seasonal mean composite wind (in  $\text{m sec}^{-1}$ ) at 500 hPa for DJF in (a) El Niño (b) La Niña and (c) El Niño minus La Niña years.

RegT-Band  
Composite Seasonal wind at 500 hPa (m/sec)

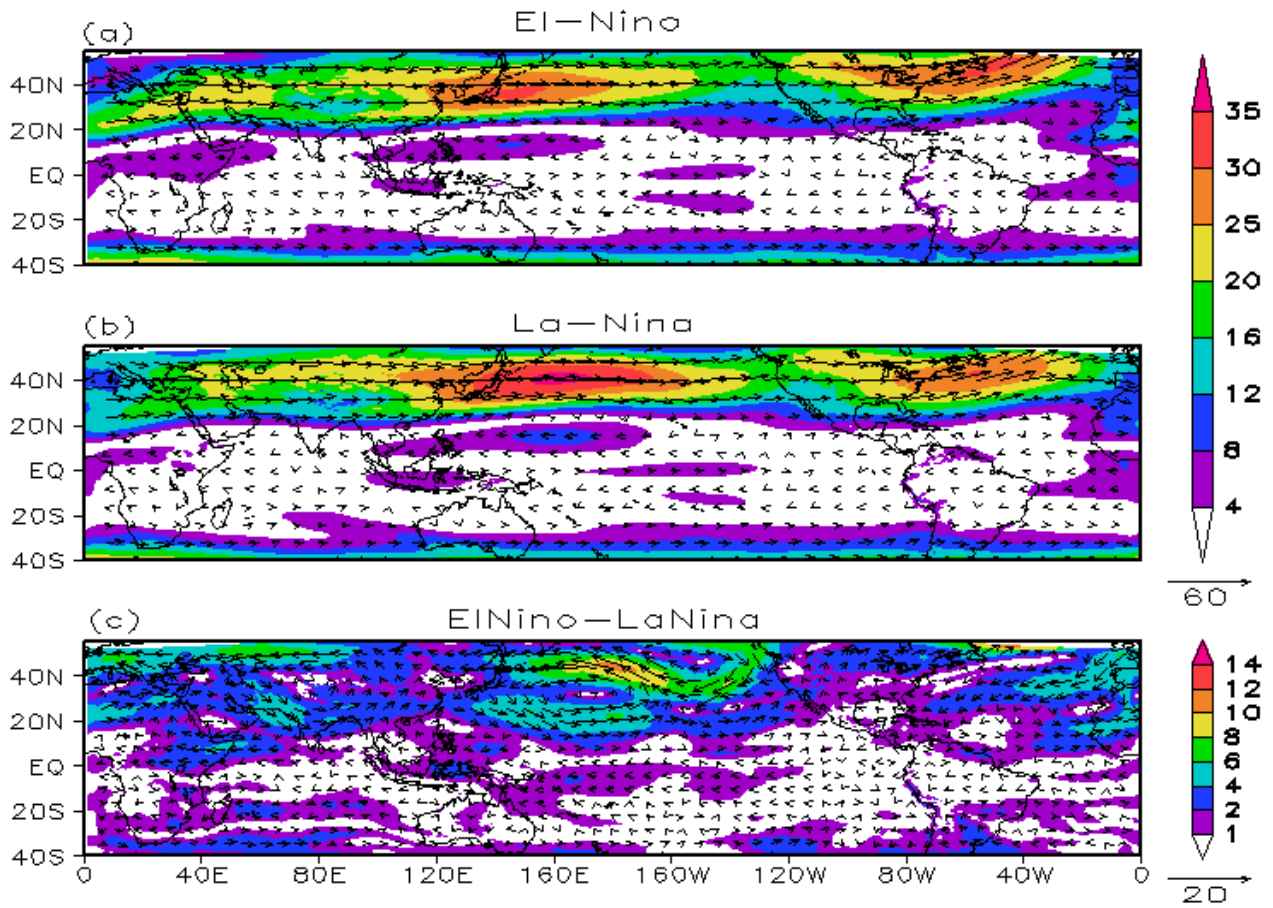


Figure 3: RegT-Band simulated seasonal mean composite wind (in  $m\ sec^{-1}$ ) at 500 hPa for DJF in (a) El Niño (b) La Niña and (c) El Niño minus La Niña years.

El Niño  
Composite Seasonal Precipitation (mm/day)

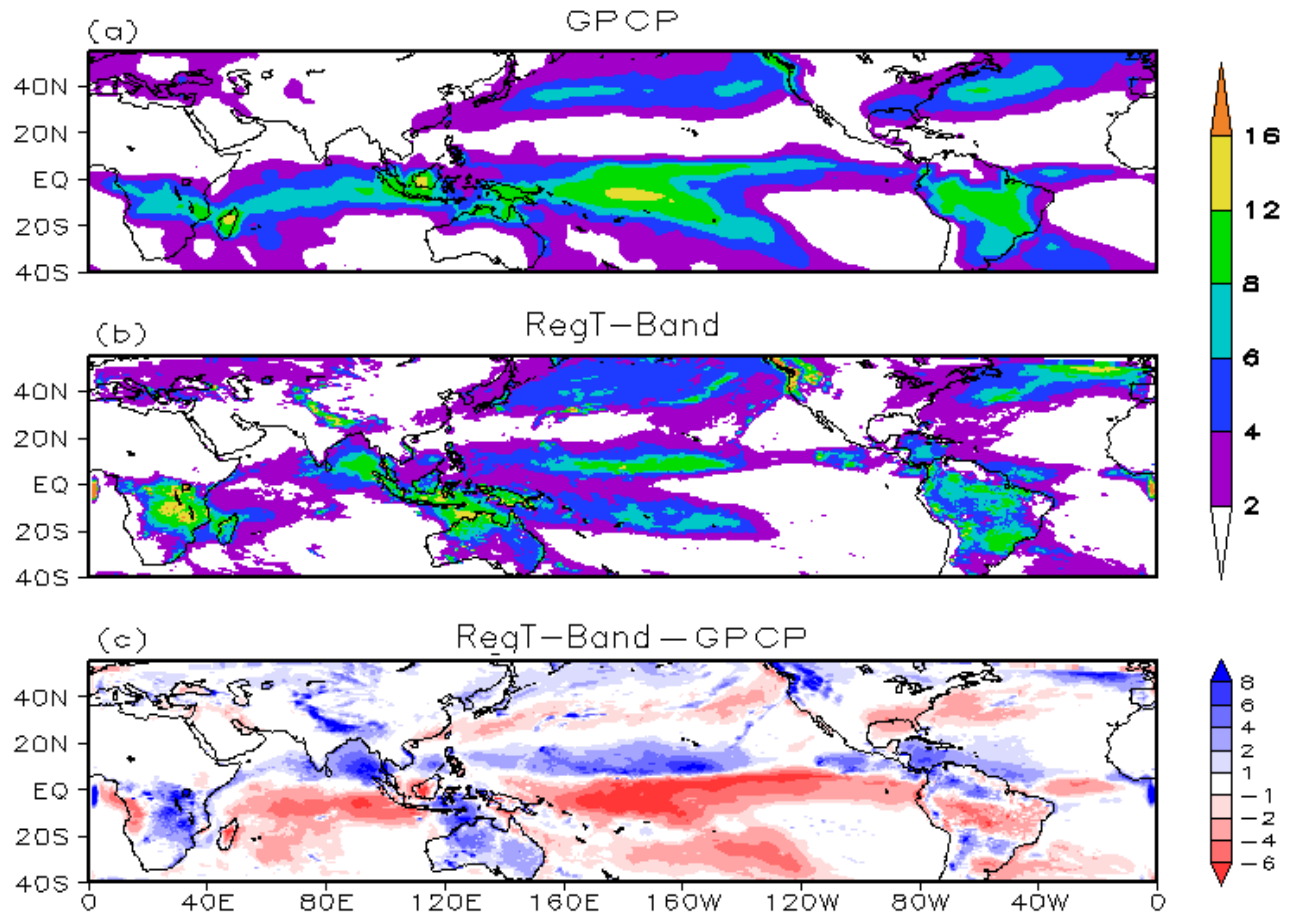


Figure 4: Seasonal mean composite (El Niño years) precipitation (in  $\text{mm day}^{-1}$ ) for DJF in (a) GPCP (b) RegT-Band and (c) difference between RegT-Band and GPCP.

La Niña

Composite Seasonal Precipitation (mm/day)

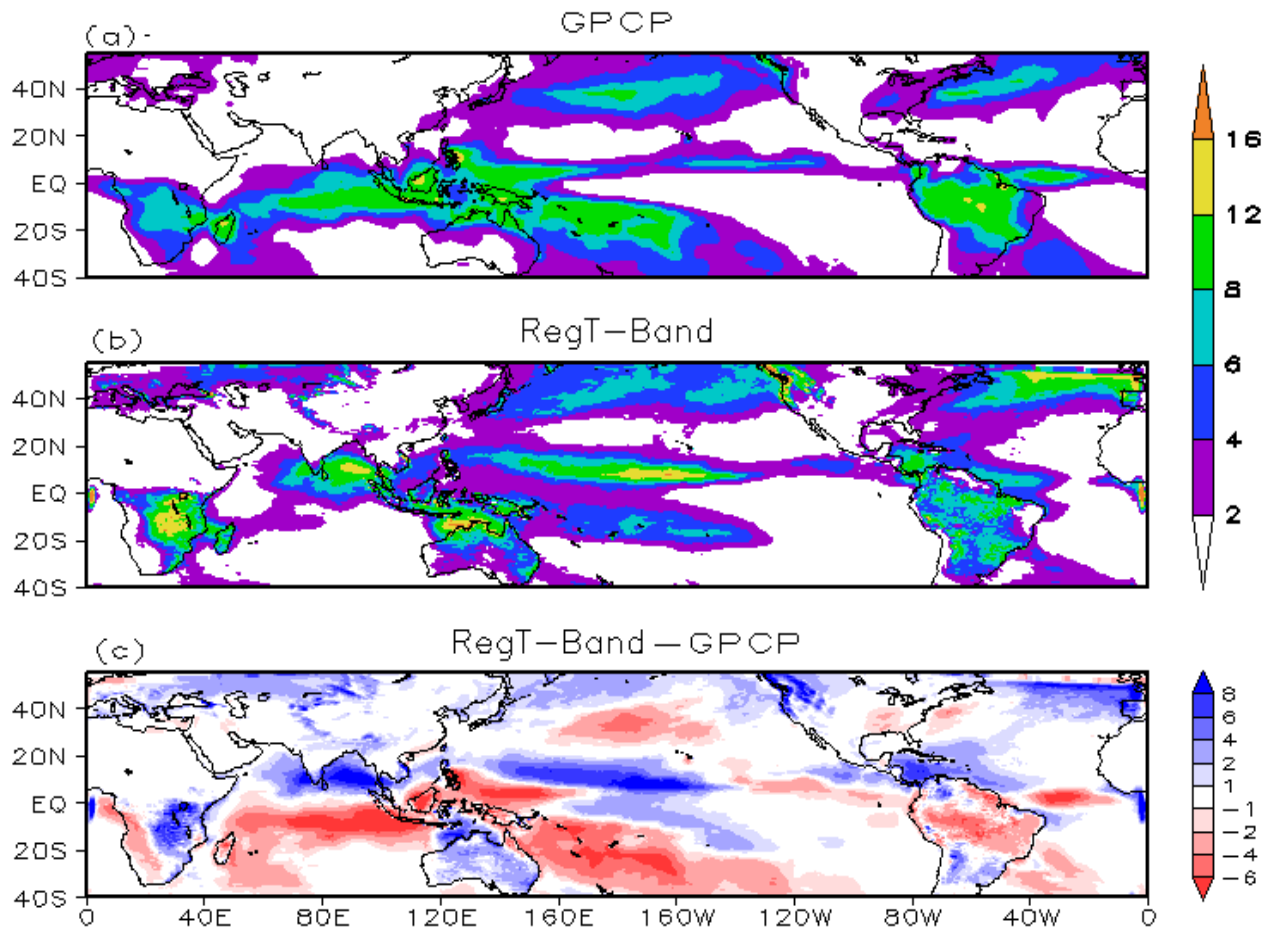


Figure 5: Seasonal mean composite (La Niña years) precipitation (in  $\text{mm day}^{-1}$ ) for DJF in (a) GPCP (b) RegT-Band and (c) difference between RegT-Band and GPCP.

## Composite Precipitation Difference (mm/day)

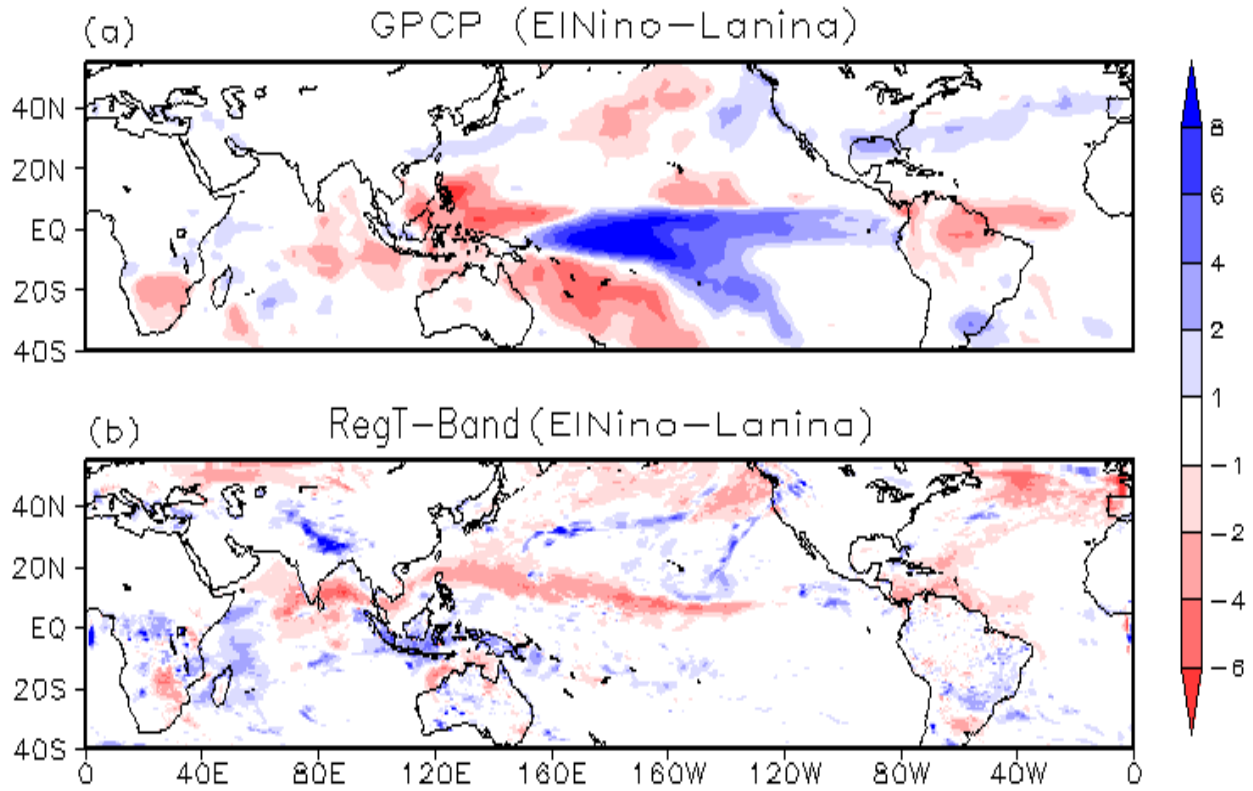


Figure 6: Seasonal mean composite (El Niño minus La Niña years) precipitation difference (in mm day<sup>-1</sup>) for DJF in (a) GPCP and (b) RegT-Band.

### box-and-whisker plot

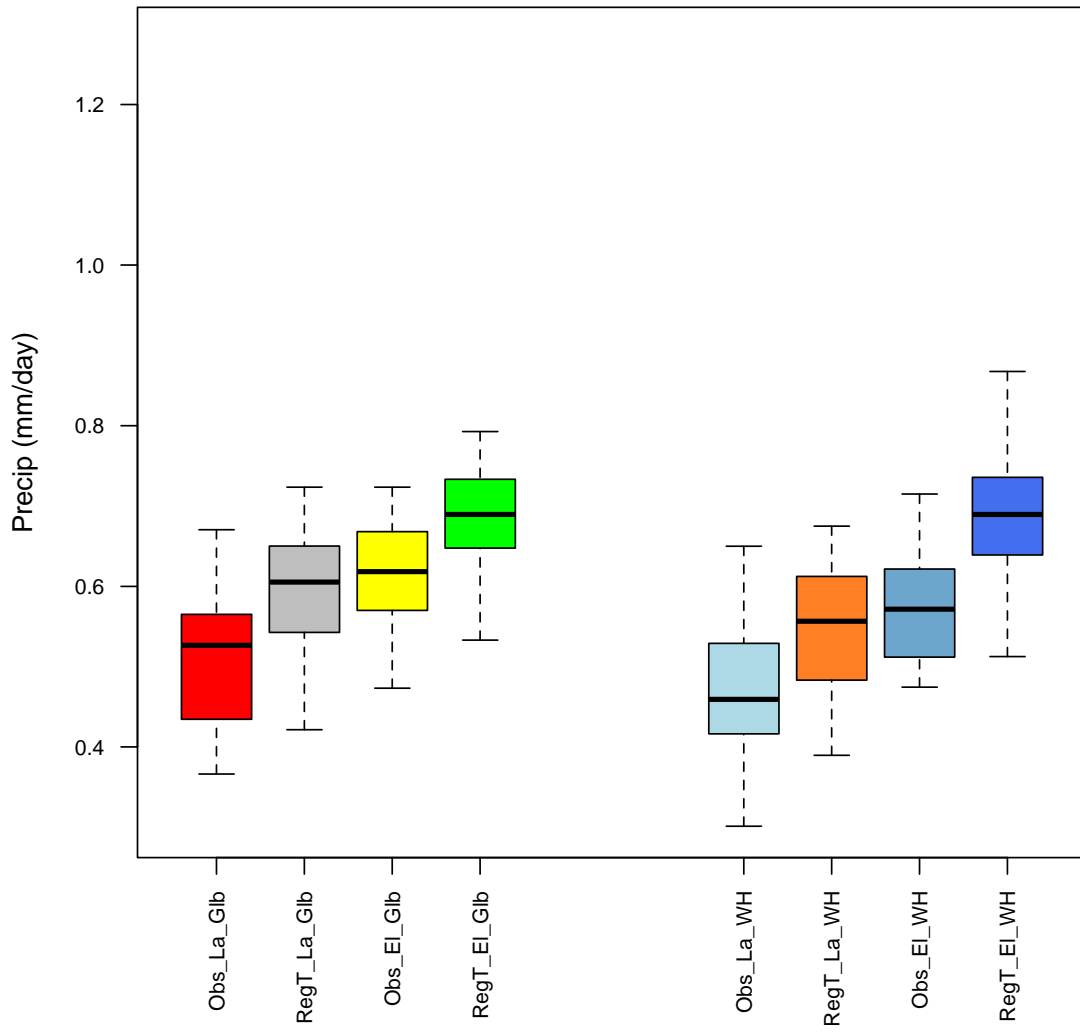


Figure 7: Distributions of observed and RegT-Band model simulated precipitation (mm/day) for El Niño and La Niña years.

### Walker Cell

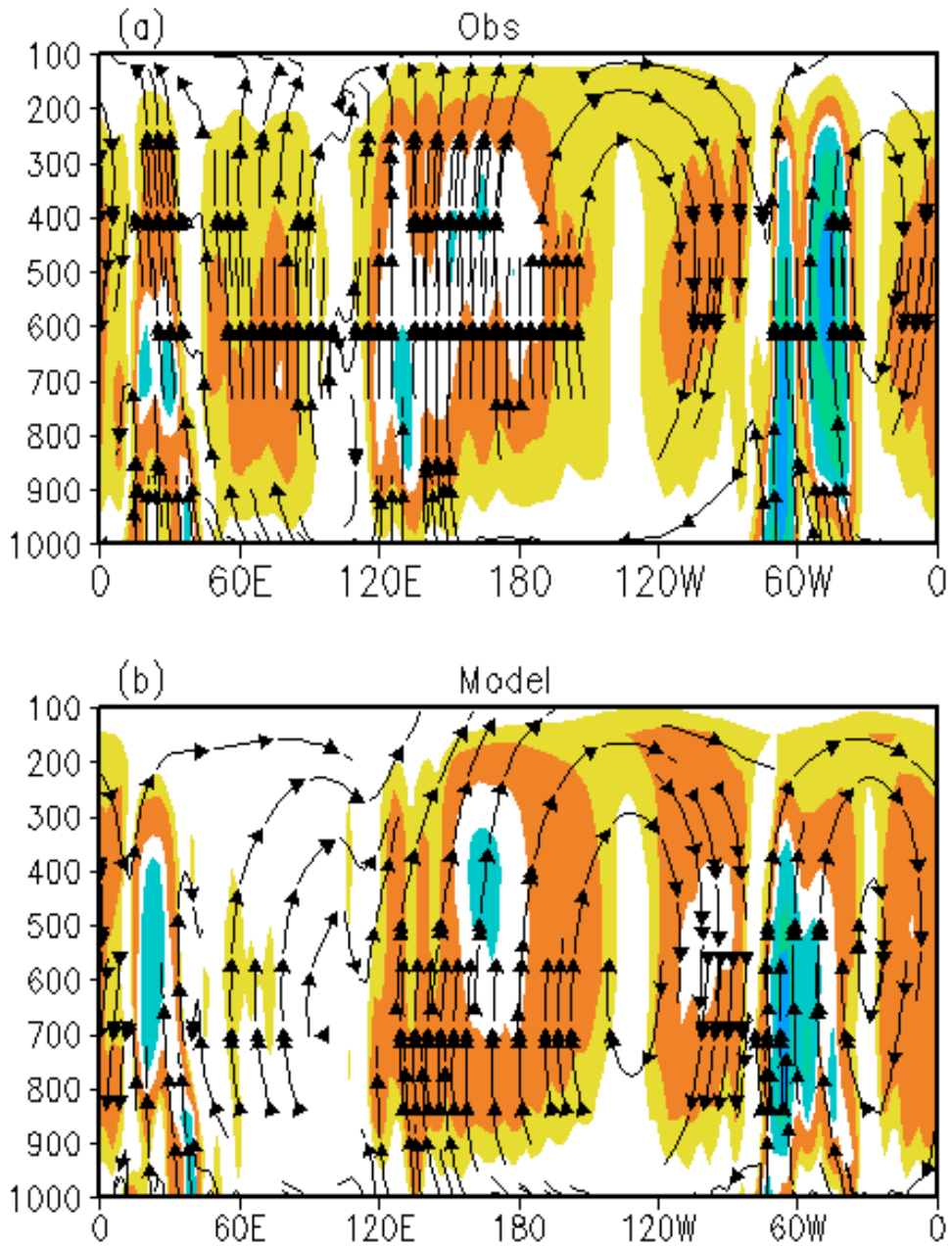


Figure 8: Composite (El Niño years) of Omega (vertical velocity) and zonal wind at pressure levels 1000 to 100 hPa for (a) Observation, (b) RegT-Band during DJF to show the Walker circulation represented by zonal wind and omega (multiplied by 600) averaged between 10° S and 10° N.

# Hadley Cell

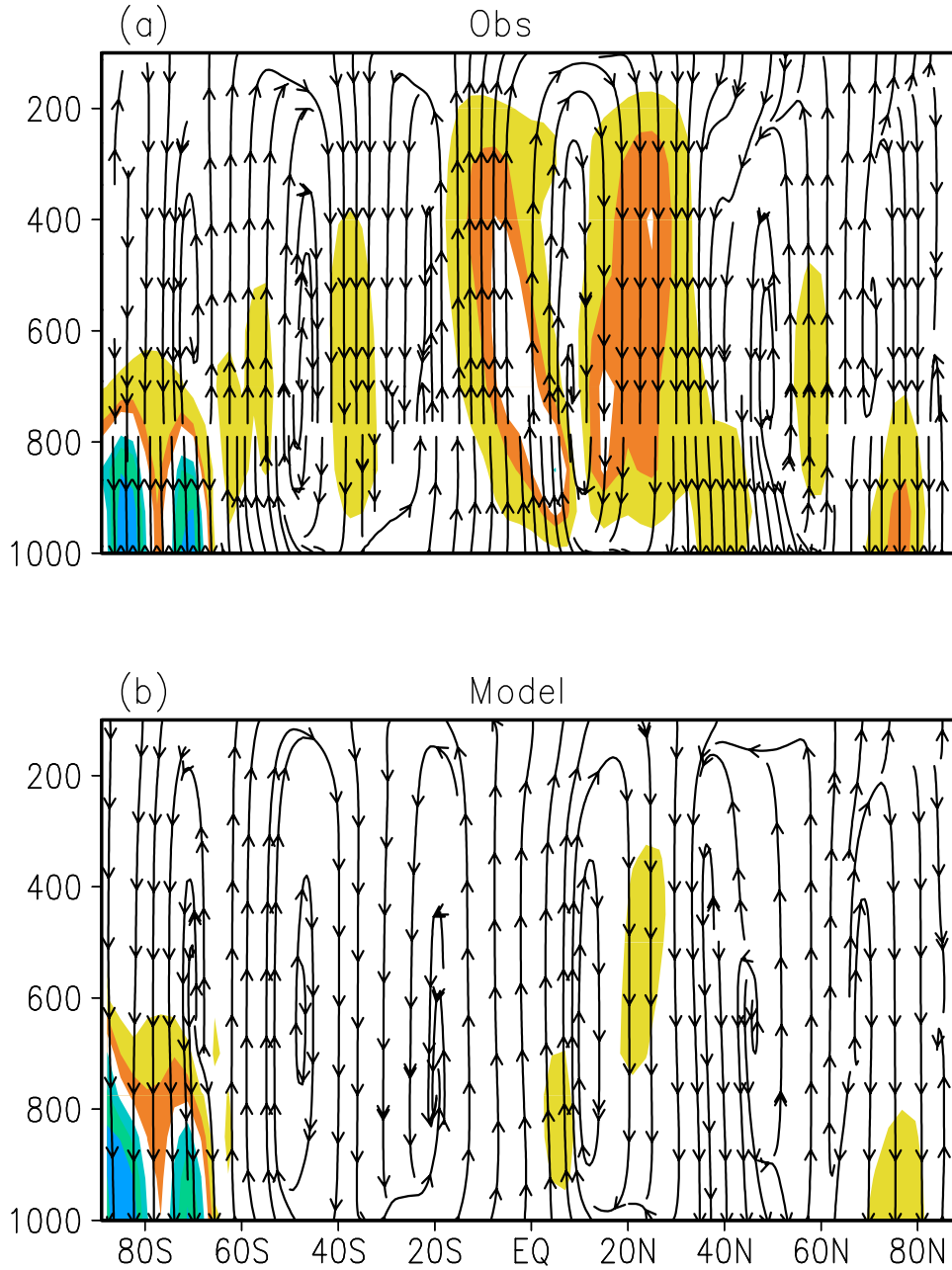


Figure 9: Composite (El Niño years) of Omega (vertical velocity) and meridional wind at pressure levels 1000 to 100 hPa for (a) Observation, (b) RegT-Band during DJF to show the Hadley circulation represented by meridional wind and omega (multiplied by 600) averaged between 28°E and 128°E.

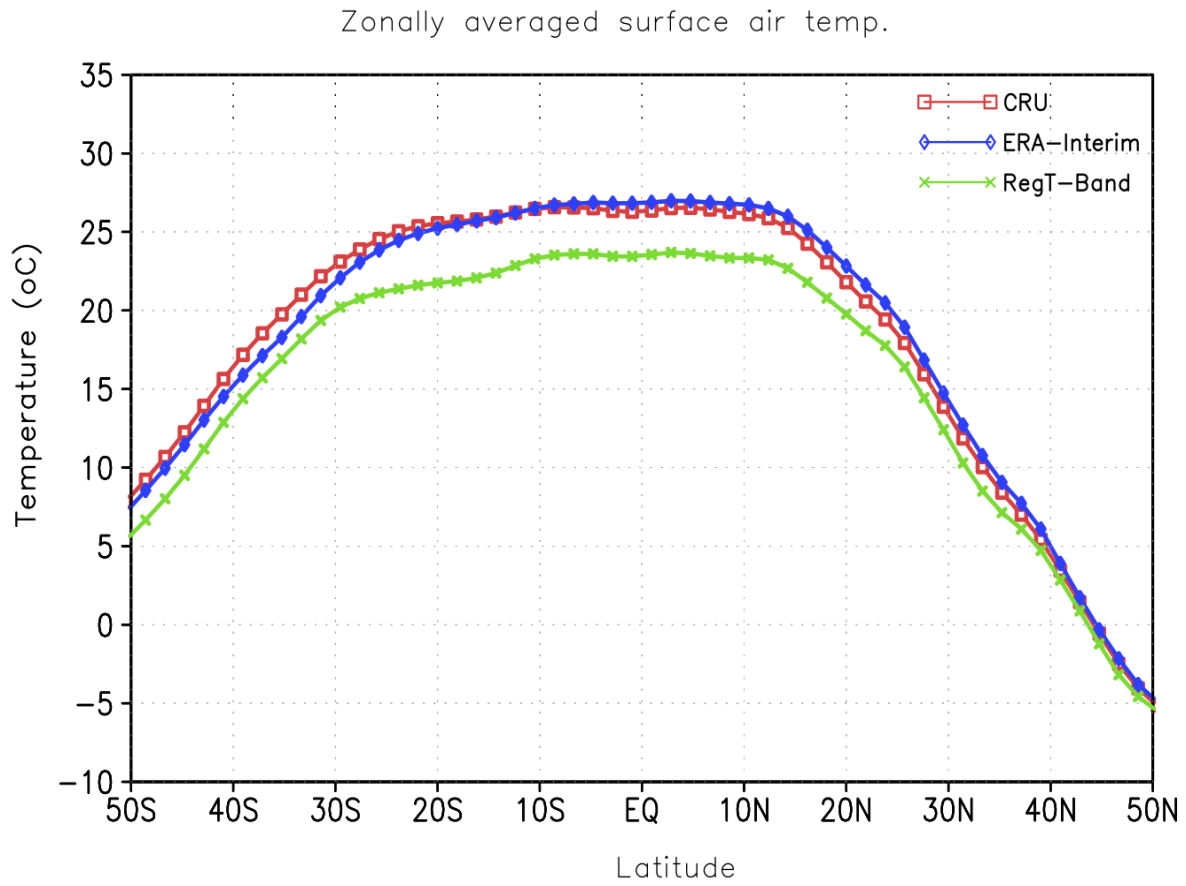


Figure 10. Seasonal mean (DJF) zonally averaged surface air temperature for composite El Niño years.

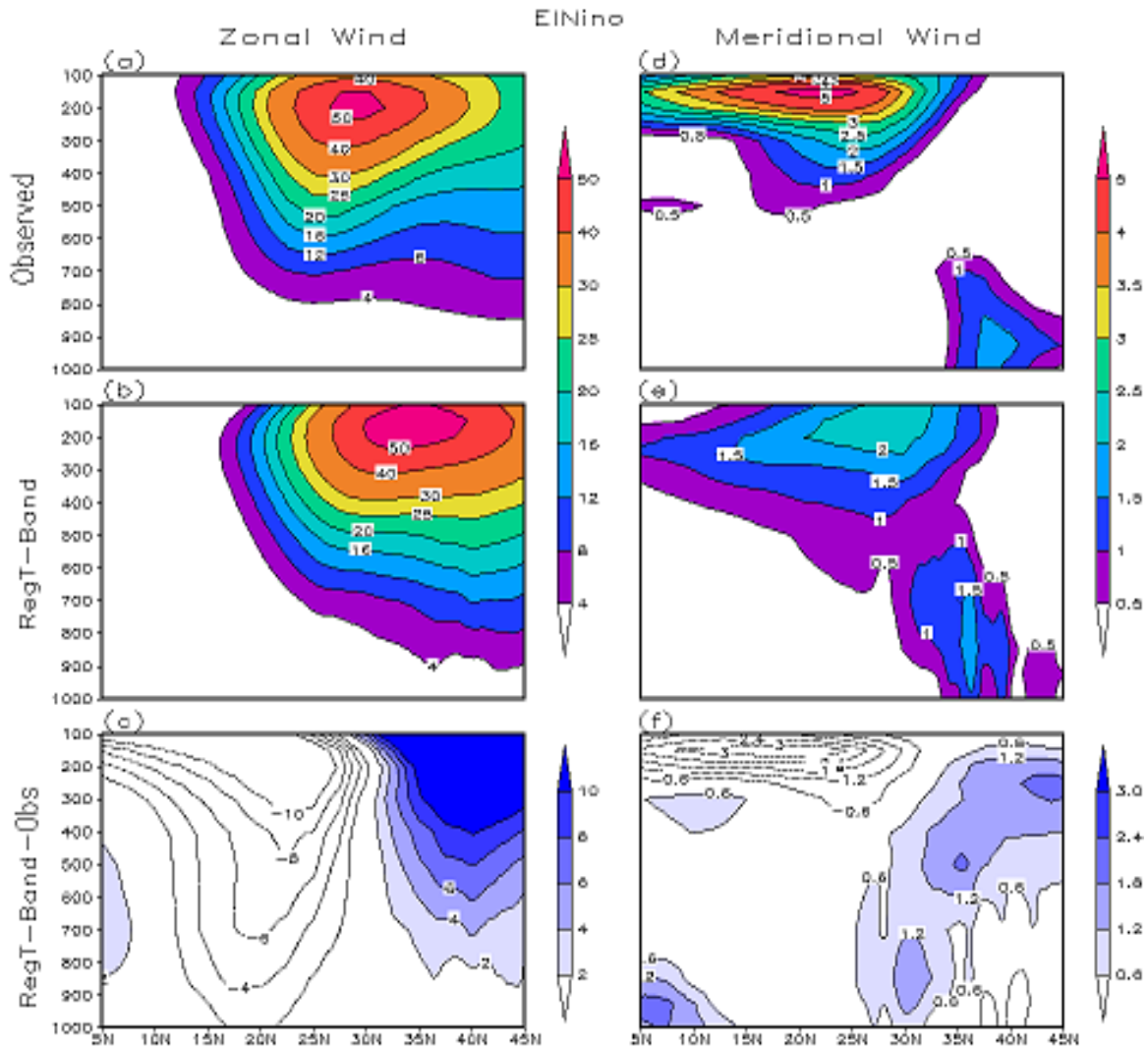


Figure 11: Sectorial (28°E-128°E) zonal seasonal mean composite wind (in  $\text{m sec}^{-1}$ ) (a) Observed, (b) RegT-Band, (c) RegT-Band minus observed precipitation; Sectorial (28°E-128°E) meridional seasonal mean composite wind (in  $\text{m sec}^{-1}$ ) (d) Observed, (e) RegT-Band and (f) RegT-Band minus observed precipitation for El Niño years.

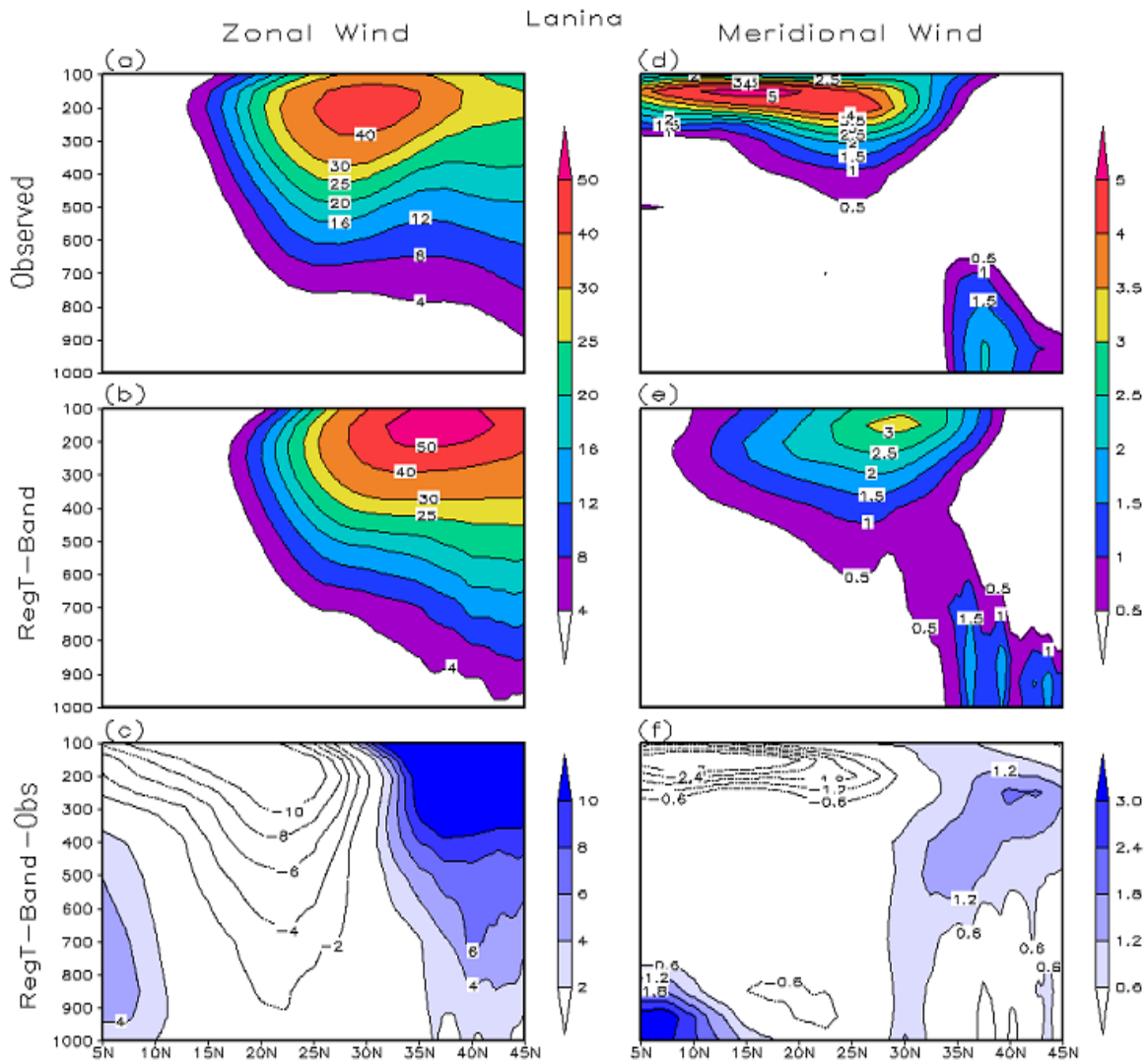


Figure 12: Sectorial (28°E-128°E) zonal seasonal mean composite wind (in  $\text{m sec}^{-1}$ ) (a) Observed, (b) RegT-Band, (c) RegT-Band minus observed precipitation; Sectorial (28°E-128°E) meridional seasonal mean composite wind (in  $\text{m sec}^{-1}$ ) (d) Observed, (e) RegT-Band and (f) RegT-Band minus observed precipitation for La Niña years.

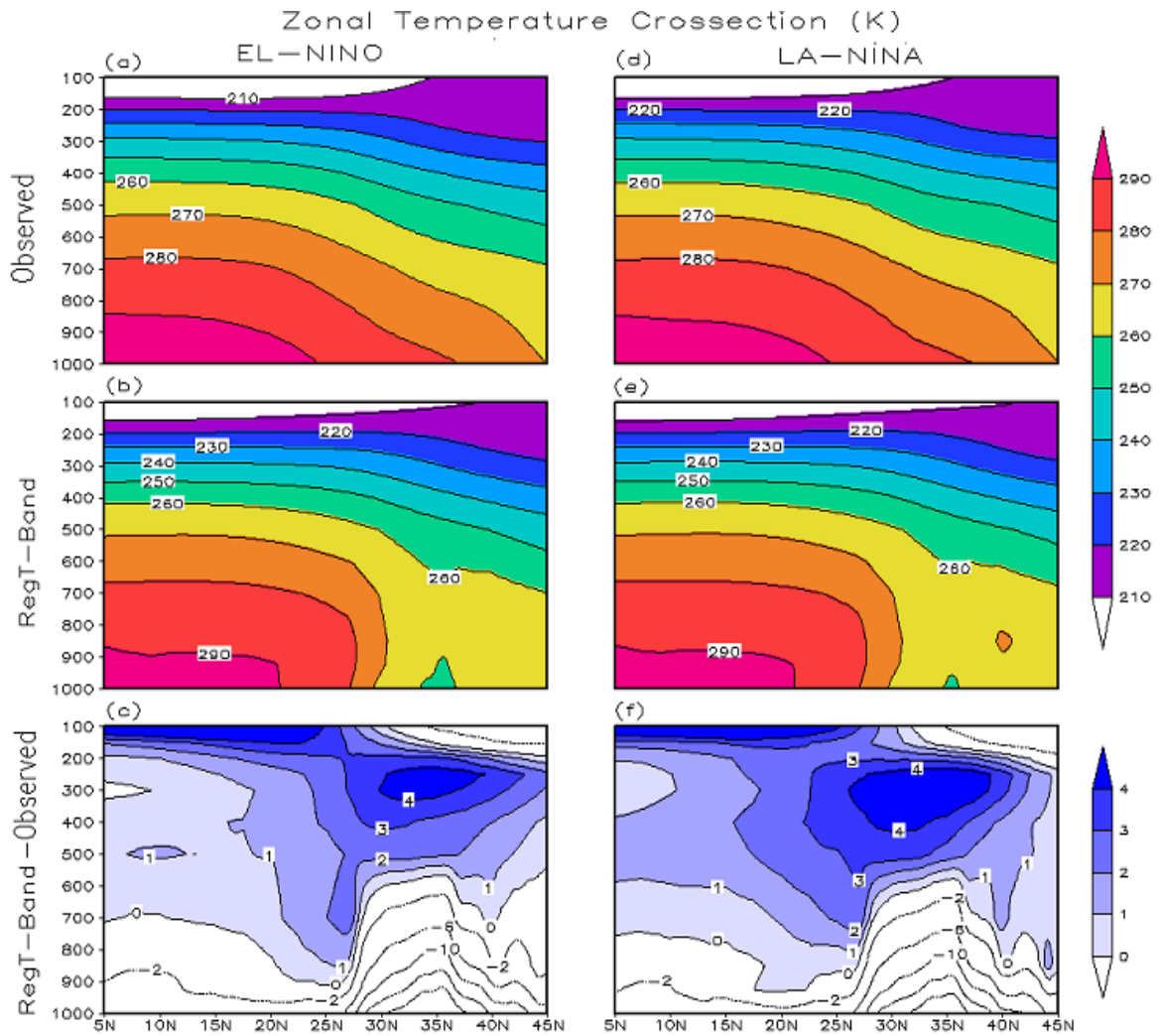


Figure 13: Sectorial (28°E-128°E) zonal seasonal mean composite temperature (in  $^{\circ}\text{K}$ ) (a) Observed, (b) RegT-Band, (c) RegT-Band minus observed precipitation for El Niño years; (d) Observed, (e) RegT-Band and (f) RegT-Band minus observed precipitation for La Niña years.

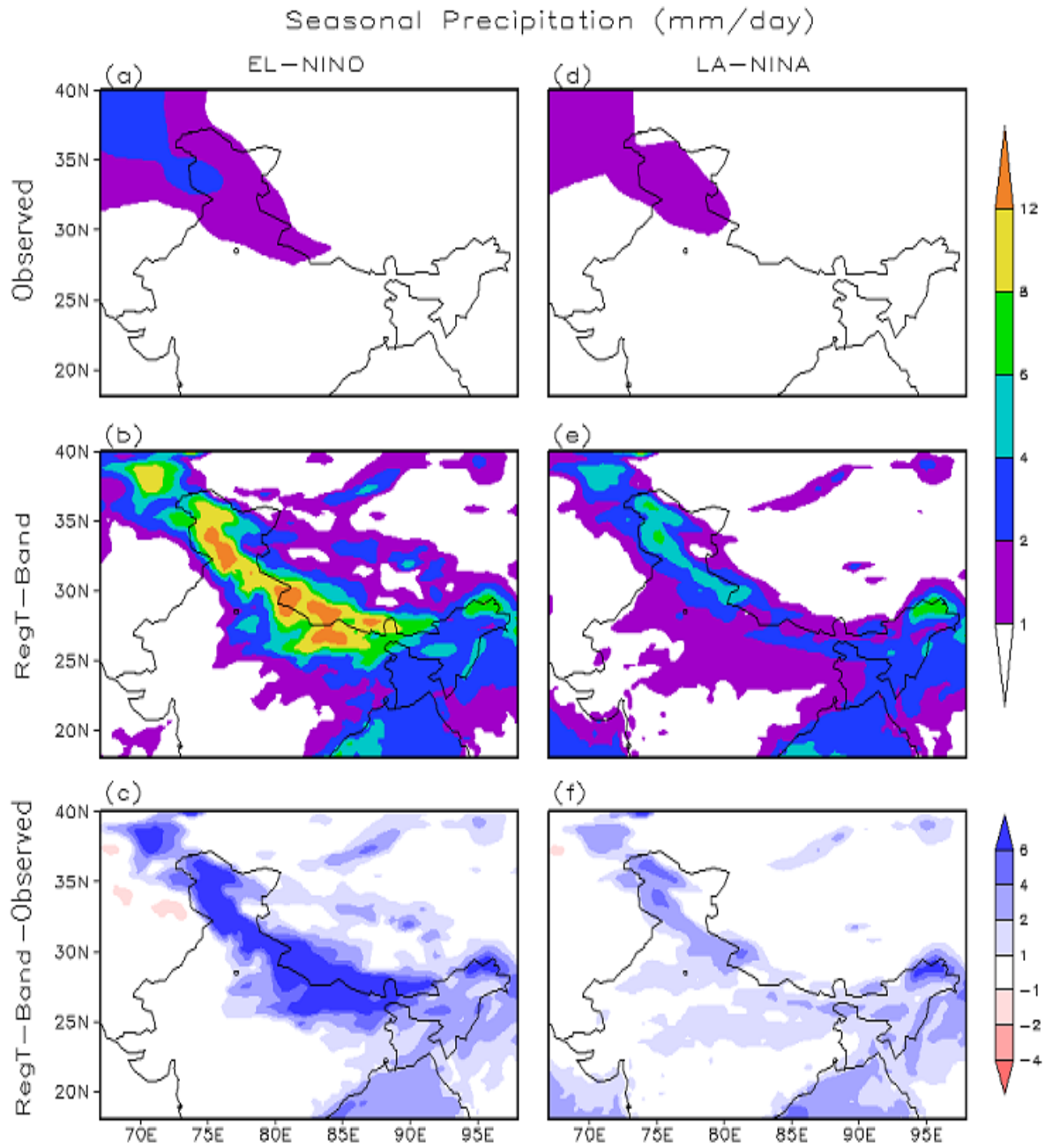


Figure 14: Seasonal mean composite precipitation (in  $\text{mm day}^{-1}$ ) (a) Observed, (b) RegT-Band, (c) RegT-Band minus observed precipitation for El Niño years; (d) Observed, (e) RegT-Band and (f) RegT-Band minus observed precipitation for La Niña years.

# Hovmoller diagram (El Niño)

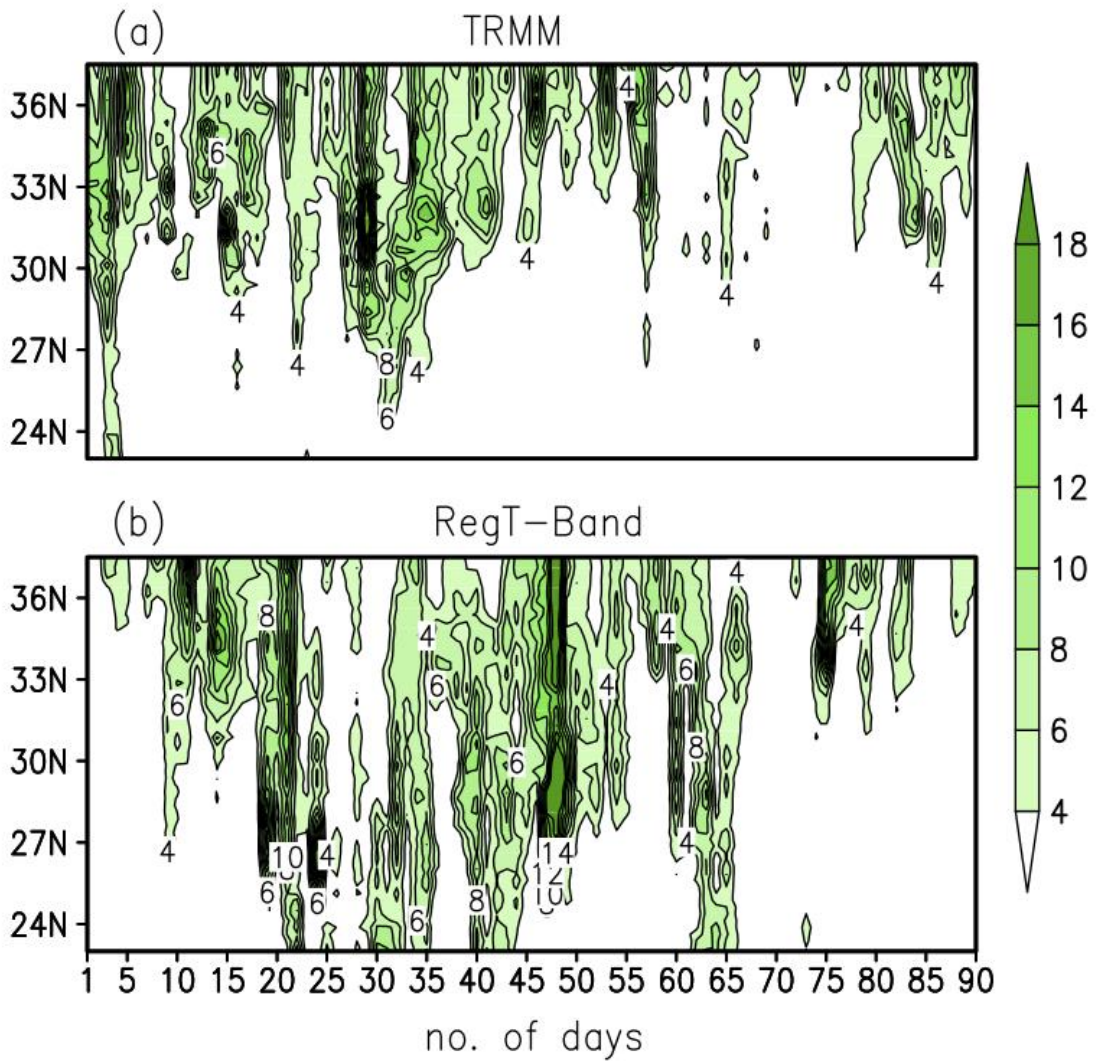


Figure 15. Hovmoller precipitation diagram for the El Niño year (2009-10) over the north India for (a) TRMM and (b) RegT-Band model.

### Hovmoller diagram (LaNina)

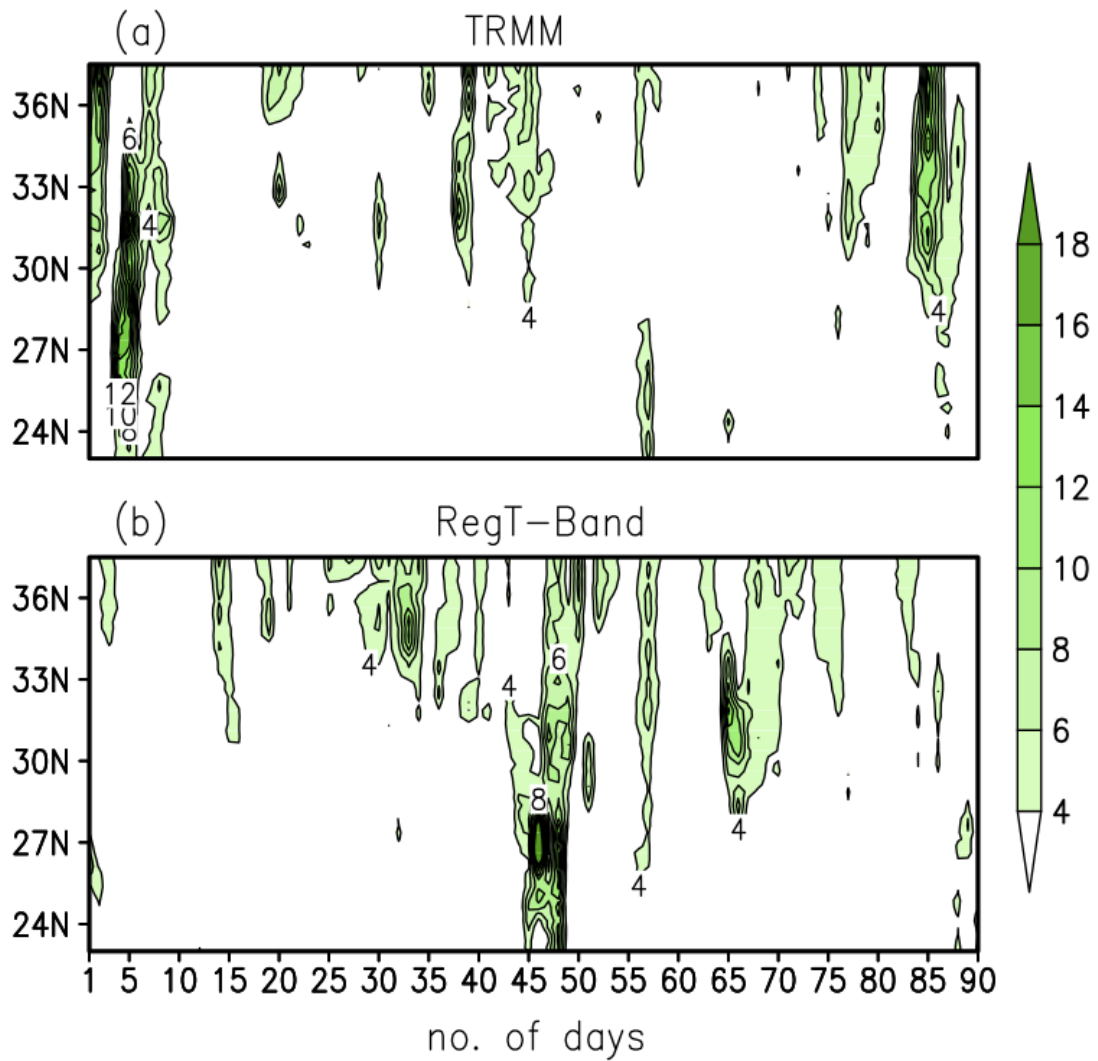


Figure 16. Hovmoller precipitation diagram for the La Niña year (2000-01) over the north India for (a) TRMM and (b) RegT-Band model.

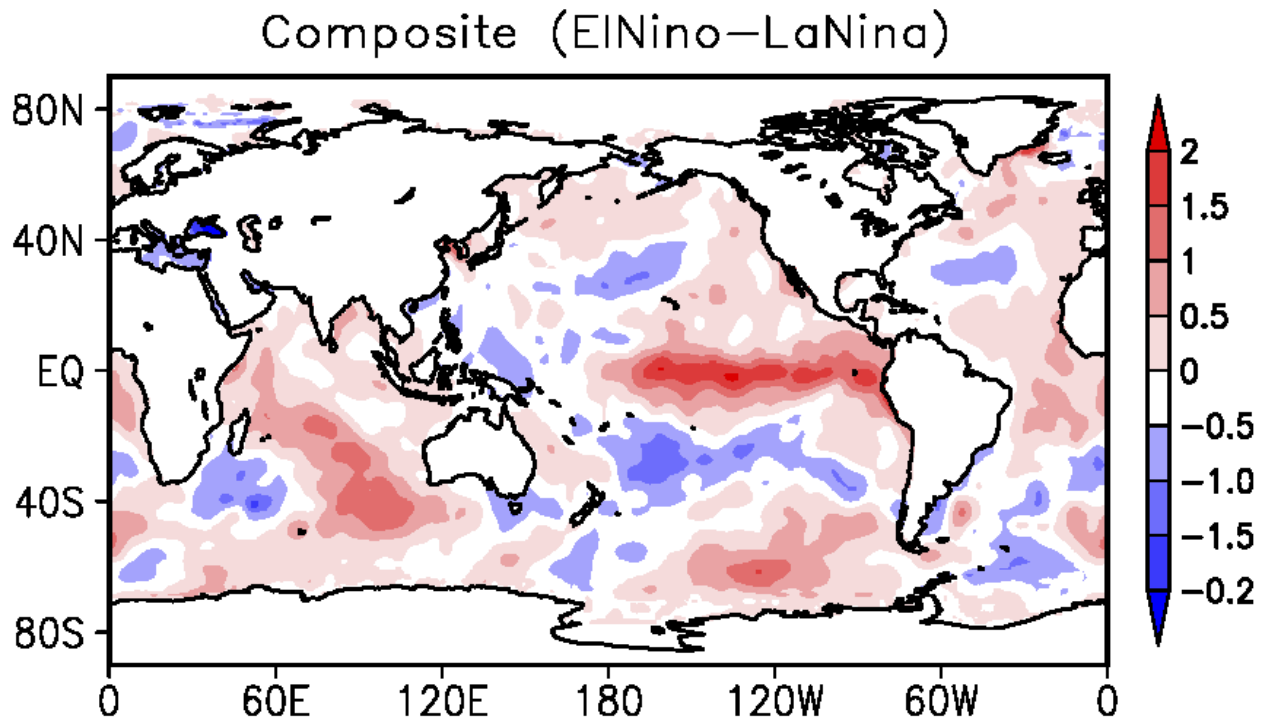


Figure 17: Seasonal mean (DJF) composite (El Niño minus La Niña years) for observed SST (in  $^{\circ}\text{C}$ ).

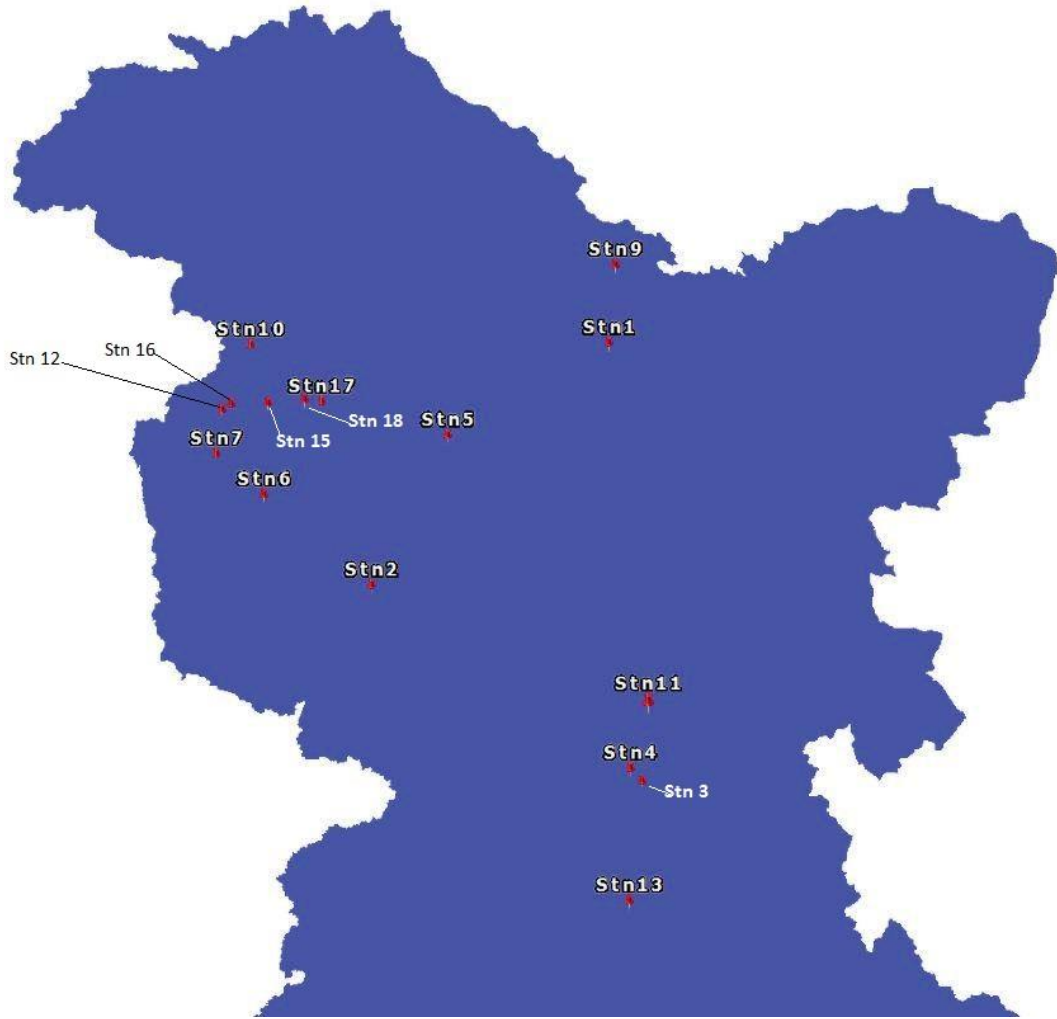


Figure 18: Seventeen station locations obtained from Snow and Avalanche Stud Establishment (SASE). These station observations of precipitation are used for validation of model results.

Table 1: Configuration of RegT-Band model used in the present study

Dynamics	Hydrostatics
Main Prognostic Variables	u, v, t, q and p
Model domain	50°S – 50°N; 180°W – 180°E; Res.= 45 km
Map projection	Mercator
Vertical co-ordinate	Terrain-following sigma co-ordinate
Cumulus convection	Grell with Fritch & Chappell closure (Grell 1993; Fritch and Chappell 1980)
Land surface processes	CLM3.5 (Oleson <i>et al.</i> 2008; Tawfik and Steiner 2011)
Planetary boundary layer	Holtlag <i>et al.</i> (1990)
Radiation parameterization	NCAR/CCM3 radiation scheme (Kiehl <i>et al.</i> 1996)

Table 2: Seasonal Mean precipitation over seventeen (17) stations obtained from SASE observation and RegT-Band simulations for El Nino and La Nina years.

Station Name (number)	Composite El Niño		Composite La Niña	
	SASE	Model	SASE	Model
1. Bahadur	2.98	4.16	2.31	2.98
2. Banihal	5.00	5.71	2.78	3.41
3. Bhang	4.75	5.69	3.83	4.37
4. Dhundi	8.15	9.87	5.70	7.18
5. Dras	2.33	3.81	1.60	3.41
6. Gulmarg	4.71	6.39	4.27	6.12
7. H-Taj	7.36	8.12	4.57	5.17
8. Kanzalwan	5.50	6.86	5.77	4.61
9. Kumar	1.55	3.74	0.93	3.56
10. Neeru	4.03	6.61	2.63	4.21
11. Patsio	3.28	5.38	2.50	3.69
12. Pharki	8.10	7.62	5.36	4.74
13. Solang	5.70	7.16	4.45	6.23
14. Stg-II	7.73	10.53	4.60	5.81
15. Z-Gali	6.37	7.47	4.30	3.19
16. Gugaldhar	5.34	5.03	2.25	4.16
17. Dawar	4.52	7.15	3.75	4.93